
DESIGN OF TARGETED COMMUNITY-BASED RESOURCE ALLOCATION IN THE PRESENCE OF VACCINE HESITANCY VIA A DATA-DRIVEN COMPARTMENTAL STOCHASTIC OPTIMIZATION MODEL

A PREPRINT

Hieu Bui

Department of Industrial Engineering
University of Arkansas
Fayetteville, AR 72701

Sandra Ekşioğlu*

Department of Industrial Engineering
University of Arkansas
Fayetteville, AR 72701

Rubén Proaño

Department of Industrial and Systems Engineering
Rochester Institute of Technology
Rochester, NY 14623

Haoming Shen

Department of Industrial Engineering
University of Arkansas
Fayetteville, AR 72701

May 10, 2024

ABSTRACT

Vaccines have proven effective in mitigating the threat of severe infections and deaths during outbreaks of infectious diseases. However, the reluctance or refusal to get vaccinated, known as vaccine hesitancy (VH), presents a significant challenge in predicting the spread of the disease and assessing the need for healthcare resources in different regions and population groups. We propose a modeling framework that integrates an epidemiological compartmental model that captures the spread of an infectious disease within a multi-stage stochastic program (MSP) that determines the allocation of critical resources under uncertainty. The proposed compartmental MSP model adaptively manages the allocation of resources to account for changes in population behavior toward vaccines (i.e., variability in VH), the unique patterns of disease spread, and the availability of healthcare resources over time and space. The compartmental MSP model allowed us to analyze the price of fairness in resource allocation. We developed a case study using real-life data about COVID-19 vaccination uptake from January to May 2021 and data about healthcare resources in Arkansas, U.S. Using our numerical analysis, we observed that (i) delaying the initial deployment of additional ventilators (critical resource) by one month could lead to an average increase in the expected number of deaths by 285.41/month, highlighting the importance of prompt action; (ii) each additional ventilator in the initial stockpile and in supply lead to a decrease in the expected number of deaths by 1.09/month and 0.962/month, respectively, highlighting the importance of maintaining a large stockpile and scalable production response; (iii) the price of ensuring equitable allocation of resources changes over time and space. This price is highest during the peak of a disease outbreak and in highly populated regions. In summary, this study highlights the importance of flexible and informed decision-making in public health crises, and the crucial role of advanced planning and preparedness for future outbreaks, offering a framework for effective resource allocation adaptable to various public health emergencies.

Keywords compartmental model in epidemiology, compartmental multi-stage stochastic program, decision making under uncertainty, resource allocation, vaccine hesitancy

*Corresponding author

1 Introduction

Infectious disease outbreaks with high reproduction numbers (R_0), such as Measles ($R_0 = 16$), COVID-19 ($R_0 \in [1.35, 2.11]$), etc., can affect a large portion of the population in a short period of time [Sy et al., 2021]. Therefore, the implementation and effective execution of public health strategies, such as vaccination campaigns, mask mandates, and social distancing, can greatly reduce the spread of the disease and save lives [Moghadas et al., 2021, Brooks and Butler, 2021, Chu et al., 2020]. However, the success of vaccination campaigns, which are crucial to controlling disease outbreaks, is often impeded by vaccine hesitancy (VH). This reluctance or refusal to get vaccinated leads to a disparity in vaccination rates and prolongs the repercussions of the disease, as in the case of the COVID-19 pandemic. Furthermore, VH complicates the prediction of vaccine demand and the allocation of critical resources [Blasioli et al., 2023].

Making well-informed and timely decisions is essential to effectively manage disease outbreaks. Compartmentalized epidemiological models, like the susceptible-infectious-recovered (SIR) and susceptible-exposed-infectious-recovered (SEIR), play a critical role in forecasting the progression of infectious diseases, thus aiding in the design of containment strategies. The SIR model divides the population into three groups: Susceptible, Infectious, and Recovered, offering a basic framework for the dynamics of the disease [Kermack et al., 1927]. The SEIR model expands on this by including an ‘Exposed’ group, which is crucial for understanding the progression of diseases that have a latency period, such as COVID-19. These models provide insight into disease transmission patterns that are vital to planning and implementing public health responses [Kong et al., 2022, Xiang et al., 2021]. The traditional SIR and SEIR models typically assume constant transition rates between compartments, such as infection and recovery rates, yet this simplification does not always hold true. Advanced models address this by incorporating the uncertainty of these model parameters. However, even these adaptations of the SEIR model that utilize stochastic compartments to inform COVID-19 strategies often neglect critical aspects of healthcare capacity and VH [Buonomo et al., 2022, Mesa et al., 2023]. Several researchers use operations research (OR) models to determine resource allocation strategies, which are critical decisions for healthcare management during disease outbreaks. These models are used to optimize the distribution of limited resources, such as ventilators during the COVID-19 pandemic, ensuring effective utilization [Mehrotra et al., 2020, Bhavani et al., 2021, Koonin et al., 2020, Bertsimas et al., 2021]. From the wide range of OR models, stochastic programming (SP) and multi-stage stochastic program (MSP) provide a robust framework for adaptive decision-making under uncertainty [Birge and Louveaux, 2011].

Incorporating dynamic disease progression data from compartmental models would significantly enhance the effectiveness of both the SP and MSP models. However, the integration of these models has been impeded by the computational challenges associated with solving each of them. Only a few studies have attempted to integrate these models to enhance the quality of resource allocation decisions [Yin and Buyuktahtakin, 2021a, Yin et al., 2023]. By incorporating the predictive power of compartmental models into SP and MSP models, we can identify and evaluate resource allocation strategies that are informed by the specifics of disease spread and progression and the availability of healthcare resources. This realization leads to our first research question (RQ1): *“Can we develop an effective resource allocation model of critical resources needed during disease outbreaks?”* To demonstrate how we can tackle this, we develop an MSP compartmental model for the COVID-19 pandemic. We first develop a compartmental model that is an extension of the SEIR model to capture the specific dynamics of the spread of the COVID-19 virus, the impact of VH on the number of people exposed, and the availability of healthcare resources on the expected number of people recovered and of deaths. The outcomes of the modified SEIR model are incorporated in an MSP model that determines resource allocation.

During disease outbreaks and other health emergencies, resource allocation becomes a critical concern. For example, the COVID-19 pandemic caused an urgent demand for essential medical equipment, such as ventilators for people in critical condition and personal protective equipment. Recognizing the gravity of the situation, the U.S. government invoked the Defense Production Act (DPA), urging car manufacturers to pivot their production lines to manufacture ventilators [Albergotti and Siddiqui, 2020]. This proactive measure showcased the influence of government interventions in crisis management. However, it also prompts reflection on its execution and raises questions such as: Could different results have been achieved with an earlier or more intensive intervention? As we anticipate and prepare for potential future outbreaks, it becomes imperative to assess the timing and intensity of interventions on healthcare outcomes. This leads to the following research question (RQ2): *“What should be effective resource allocation strategies at the start of an outbreak?”* Specifically, how does the timing and scope of interventions, such as DPA, impact the spread of the disease? How does VH impact the effectiveness of resource allocation? By exploring this research question, our aim is to provide guidance on optimizing resource allocation strategies to ensure that they are timely and effective.

Ensuring access to healthcare resources is crucial, especially during disease outbreaks, since strategies used for resource allocation can have significant impacts on the affected population. Several OR models take a utilitarian ap-

proach by focusing on minimizing costs or maximizing the benefits from the allocation of limited healthcare resources. Such an approach allocates resources to highly populated areas and those that have access to healthcare care, which may lead to inequity. In the U.S., access to healthcare varies greatly, and rural and marginalized communities often face more challenges in accessing the necessary services and resources [Mishra et al., 2021]. These disparities can affect the effectiveness and success of public health intervention strategies. This leads to our next research question (RQ3): “*What are the trade-offs between equity, equality, and the effectiveness of resource allocation?*” Exploring this question will help to understand how resource allocation strategies influence disease outbreak management, both in the short and long term.

2 Literature review

We identified three streams of literature related to our research: compartmental models in epidemiology, stochastic optimization models for resource allocation, and modeling equity in healthcare. The first stream of literature focuses on compartmental models, such as the SIR and SEIR. These models categorize populations into different subgroups according to their health status. These models provide a structured approach to assess disease progression and assess the impact of interventions on the affected population. The second stream of literature focuses on multistage stochastic programs (MSPs), models that aid in making decisions under uncertainty. Our study integrates compartmental models within an MSP framework to optimize resource allocation to manage and contain infectious diseases. The third stream addresses equity in resource allocation. The goal is to ensure a fair and accessible distribution of healthcare resources, which is vital during infectious disease outbreaks. Each of the following subsections provides a comprehensive overview of the literature. We highlight their relevance to our proposed research model.

2.1 Compartmental Models in Epidemiology

Epidemiological models are key to understanding and predicting the course of infectious disease outbreaks. With the emergence of COVID-19, the field of mathematical epidemiology quickly attracted broader interest. Taking advantage of existing approaches, researchers adapted and applied various methods specifically to study COVID-19, including compartmental models, structured metapopulations, agent-based networks, deep learning, and complex networks [Wu et al., 2020, Adiga et al., 2020, Rodríguez et al., 2021, Zhou et al., 2020a, Chang et al., 2021a, Kerr et al., 2021, Chang et al., 2021b]. Among these, compartmental models are essential in infectious disease research due to their effective representation of the dynamics of disease transmission. In these models, the population is divided into several subgroups or compartments, each representing a specific stage in the progression of the disease. Consider, for example, the SIR model that divides the population into three compartments: Susceptible, Infectious, and Recovered. This model provides a basic framework for tracking disease spread by monitoring changes in population proportions within these compartments. Building on the SIR model, the SEIR model adds an Exposed compartment, highlighting a critical phase where individuals have contracted the disease but are not yet infectious. This addition is particularly important for diseases that have an incubation period, such as COVID-19. Several researchers extended the SEIR model to capture the unique transmission dynamics of the COVID-19 virus, as well as the impacts of vaccination and public health mandates on the spread of the disease. Kong et al. (2022) provide a detailed overview of these extensions, which consider various stages of disease progression, intervention strategies, and demographic factors [Kimathi et al., 2021, Tuite et al., 2020, Foy et al., 2021].

Classic epidemiological models assume that model parameters, such as the transmission rate, the recovery rate, and the contact rate, are constant throughout the course of the epidemic being modeled. Most recently, epidemiological models have been updated to incorporate the variability and uncertainty of these parameters. Models that take into account the randomness that exists in the system can lead to better decision-making. For example, [Lekone and Finkenstädt, 2006, Gray et al., 2011, Faranda and Alberti, 2020, Ganyani et al., 2021, Maltsev and Stern, 2021, Gatto et al., 2020, Giordano et al., 2020, Kretzschmar et al., 2020, Kucharski et al., 2020] propose stochastic epidemiological models. These models use historical data to estimate how parameters change over time, and thus, provide a more realistic representation of the dynamics of infectious diseases.

VH has consistently presented a significant challenge to the healthcare system, a concern that has been recognized from the World Health Organization (WHO) as a global health threat ([WHO, 2019]. The advent of COVID-19 vaccines once again highlighted this issue. Several compartmental models capture the impact of vaccine availability and hesitancy on transmission rate. Buonomo et al. [2022] demonstrate that voluntary vaccination alone cannot stop the spread of the disease. Choi and Shim [2020] develop a game-theoretic epidemiological model to explore vaccination and social distancing as strategies to control the spread of the disease. They use a group behavioral model to determine optimal strategies for individuals. Awad et al. [2021] propose a compartmental model that uses geospatial and VH information to develop strategies to distribute vaccines. Jing et al. [2023] examine the role of VH in the emergence

of new SARS-CoV-2 variants. Bui et al. [2024] present a compartmental model that captures the impact of VH on disease outcomes, such as the expected number of hospitalizations and deaths. The model runs for different values of VH (which are taken from a certain distribution) to estimate the impacts of uncertain VH on model outcomes. The authors performed a sensitivity analysis to assess the impact of the availability of healthcare resources and vaccines on the expected number of deaths. Despite the variety of compartmental models available, none examines the impacts of the temporal and spatial variations of VH on demand for healthcare resources. This gap underscores the need for models that use predictions of temporal and spatial disease spread to determine the effective allocation of critical resources.

Based on our review of the literature, epidemiological models are typically used to support decision making via “What-if” analysis. This approach explores how changes in model parameters or assumptions affect the spread of the disease and the need for resources. Some researchers integrate epidemiological models into optimization models to support optimal decision making during disease outbreaks. For example, Abdin et al. [2023] propose a non-linear programming formulation of a compartmental model to present the complex dynamics of infectious diseases, offering a nuanced perspective on disease transmission. Yin and Buyuktahtakin [2021a] propose an MSP compartmental model to support resource allocation during the Ebola outbreak in West Africa. The MSP uses information on stochastic disease progression to determine resource allocation to control the infectious disease outbreak. The model determines the fair allocation of critical resources.

Our study investigates the impact of vaccination and VH on disease transmission dynamics. The model we propose enables decision makers to assess the impact that the timing, scale, and scope of resource allocation have on the spread of the disease and disease outcomes. While previous research has addressed aspects of resource management during disease outbreaks, none has presented a comprehensive, data-driven model, as we propose. Our model highlights the advantages of merging the predictive capabilities of compartmental models with optimization techniques, providing valuable insights into effective disease control strategies.

2.2 Stochastic Optimization Models for Resource Allocation

MSP models are used to support sequential decision making under uncertainty. The simplest MSP model, the two-stage stochastic program (2-SP), is commonly used to minimize expected costs (maximize expected benefits) in decisions made today and tomorrow in the face of uncertainties faced tomorrow. MSPs are an extension of 2-SPs, which involves making decisions sequentially based on new information that emerges over time. For an overview of SP and MSP models and their applications, we refer the reader to Pereira and Pinto [1991], Goh et al. [2007], Zhang and Cardin [2017], Li and Grossmann [2021].

MSP models pose significant computational challenges that stem from the inherent uncertainty in the data and the intricate nested structure characteristic of multistage decision-making problems. A common approach to handling uncertainty is to approximate the underlying stochastic process using a scenario tree. A scenario tree branches at each stage to consider a finite number of possible scenarios. When the number of scenarios is small, the deterministic equivalent of the MSP problem can be solved using commercial optimization solvers, such as CPLEX or Gurobi. Lagrangian and Benders decomposition methods are often used to solve problems with a large number of scenarios. These methods break down the problem into smaller subproblems that are easier to solve [Laporte and Louveaux, 1993, Guignard, 2003]. Rolling-horizon and heuristic approaches are also used to solve larger-scale MSP models [Christian and Cremaschi, 2015].

MSP models are often used for resource allocation in the healthcare sector, as the size and timing of the demand for these resources are often uncertain, and the availability of resources is limited. For example, Yin and Buyuktahtakin [2021b] develop an MSP model to effectively manage resource allocation during the 2018-2020 Ebola outbreak. In response to the COVID-19 pandemic, Yin et al. [2023] propose an MSP model for allocating ventilators across counties in New York and New Jersey. Their MSP incorporates a compartmental model to account for disease dynamics under varying levels of uncertainty. Hosseini-Motlagh et al. [2023] introduce a multi-stage fuzzy SP approach for patient allocation across healthcare facilities during COVID-19. Tanner et al. [2008] and Yarmand et al. [2014] propose SP models to determine optimal vaccination strategies. Mehrotra et al. [2020] propose an SP model for ventilator allocation during COVID-19, focusing on cost minimization. These publications highlight the relevance of MSPs to support sequential decisions related to resource allocation under uncertainty.

Integrating compartmental models within MSP resource allocation models provides a robust framework for planning responses to disease outbreaks. This approach enables high-quality decision making over time, taking into account the unpredictable nature of disease spread and resource availability. While some researchers are investigating this modeling approach, there is more to be done. Our proposed data-driven compartmental MSP model addresses VH and

fairness in resource allocation within this modeling framework. Our proposed model supports effective vaccination strategies and resource allocations that ensure greater immunity and mitigate the impact of outbreaks.

2.3 Equity in Healthcare Resource Allocation

A WHO report highlights the importance of following ethical principles in the allocation of healthcare resources by analyzing the utility, efficiency, and fairness approaches taken by decision makers [WHO, 2004]. Utilitarian decision makers implement strategies that yield the highest overall benefit or the lowest overall cost. Efficient decision makers advocate using the least amount of resources to achieve the maximum possible impact. Fair decision makers aim to ensure equitable allocation and reduce disparities between groups and individuals. Aligning resource allocation strategies with these principles can be challenging as each strategy, while meeting one principle, falls short of meeting others. The work of Lane et al. [2017] highlights the complexity of ensuring equity in allocating healthcare resources, emphasizing the need for clear definitions that reflect societal values to ensure equal access to healthcare, address patient needs effectively, and distribute potential benefits fairly. Equitable strategies can build public trust and encourage cooperation, which are essential during health crises.

Several OR models for resource allocation take a utilitarian approach to optimize logistics and operations to control disease spread [Sun et al., 2014, Liu et al., 2015, Liu and Zhang, 2016, Zaric and Brandeau, 2001, Day et al., 2020]. Other studies introduce fairness metrics and propose models that optimize fairness in resource allocation. For example, Orgut et al. [2016] proposes a model that allocates and distributes food donations proportionally to demand, aiming for an equitable distribution while minimizing waste. Similarly, Davis et al. [2015] propose a multi-step optimization approach to improve fairness in the allocation of organs (kidneys) across the U.S., thereby improving equity of organ transplant. Dönmez et al. [2022] presents a multi-objective, multi-period, nonlinear model for equitable personal protective equipment (PPE) allocation to health centers in pandemics, with the aim of minimizing infections and ensuring fair distribution amidst resource scarcity. The research by Yin and Buyuktahtakin [2021a] introduces an MSP model for a fair allocation of resources, such as beds and treatment centers, during the West African Ebola outbreak, balancing efficiency and equity in epidemic responses.

Similarly to the literature, our proposed model allows decision makers to evaluate the trade-offs between fairness and efficiency in allocating critical healthcare resources. Unique to our approach is the incorporation of uncertainty in VH, which introduces additional complexity to resource allocation strategies. We analyze the ‘price of fairness’, the efficiency loss incurred when striving for equitable resource allocation over time and across different geographic regions. The MSP compartmental model adapts to the evolving landscape of healthcare needs, ensuring that resource allocation remains responsive and equitable even under unpredictable changes in public sentiment towards vaccination.

3 Method

We propose a compartmental MSP model to evaluate how uncertainty in VH, and disease progression over time and space impact decisions about allocating healthcare resources. Section 3.1 focuses on the generation of scenarios used in the compartmental MSP model. Detailed descriptions of the compartmental model and the compartmental MSP model are presented in Sections 3.2 and 3.3, respectively.

3.1 Uncertainty representation

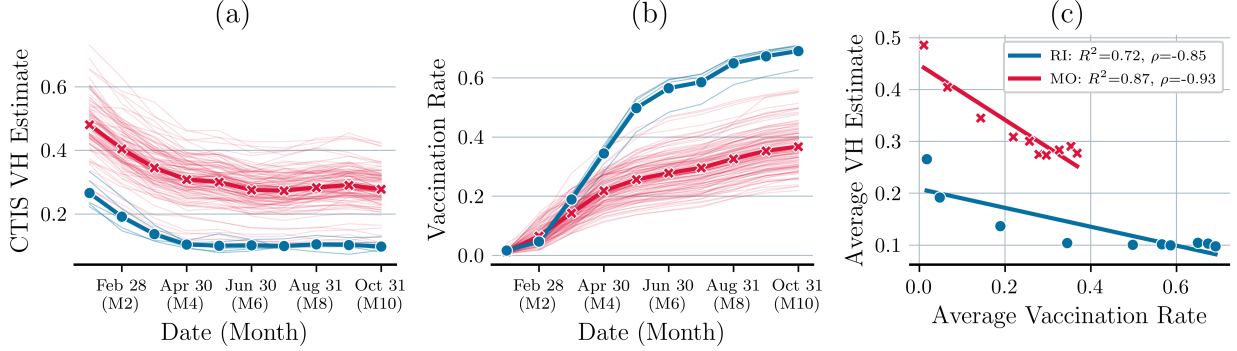
Motivation: Our proposed model considers uncertainty in VH. This is motivated by observations made from the COVID-19 Trends and Impact Survey (CTIS) conducted by the Delphi Group at Carnegie Mellon University, in collaboration with Facebook [Salomon et al., 2021], and from data about vaccination rates collected by the Centers for Disease Control and Prevention CDC [2021].

Figure 1(a) presents VH estimates of every county in the states of Missouri (MO) and Rhode Island (RI), providing a snapshot of the willingness of the public to vaccinate. The VH estimate is derived from responses to the following question in the CTIS survey: “If a vaccine to prevent COVID-19 was offered to you today, would you choose to get vaccinated?”. Participants were asked to select one of the following answers “Yes, definitely,” “Yes, probably,” “No, probably not,” or “No, definitely not.” The last three responses are considered indicative of VH. Each thin line represents VH progression of an individual county. The thicker line depicts the average VH trend for the respective state.

Figure 1(b) shows the vaccination rates in counties of Missouri and Rhode Island based on data from CDC [2021]. The data show fully vaccinated individuals who have received the complete dose - either two doses of a two-dose vaccine or one dose of a single-dose vaccine. These data highlight a general decline in VH over time and underscore the varied

vaccination sentiments in counties. Figure 1(c) illustrates a negative correlation between average vaccination rates and average VH estimates with correlation coefficients of $\rho = -0.85$ for Rhode Island and $\rho = -0.93$ for Missouri. The high correlation coefficients in both states indicate that higher vaccination rates are associated with lower VH.

Figure 1: (a) CTIS-derived vaccine hesitancy, (b) vaccination uptake trends, and (c) correlation plot between VH and vaccination rate of counties in Rhode Island (RI) and Missouri (MO).



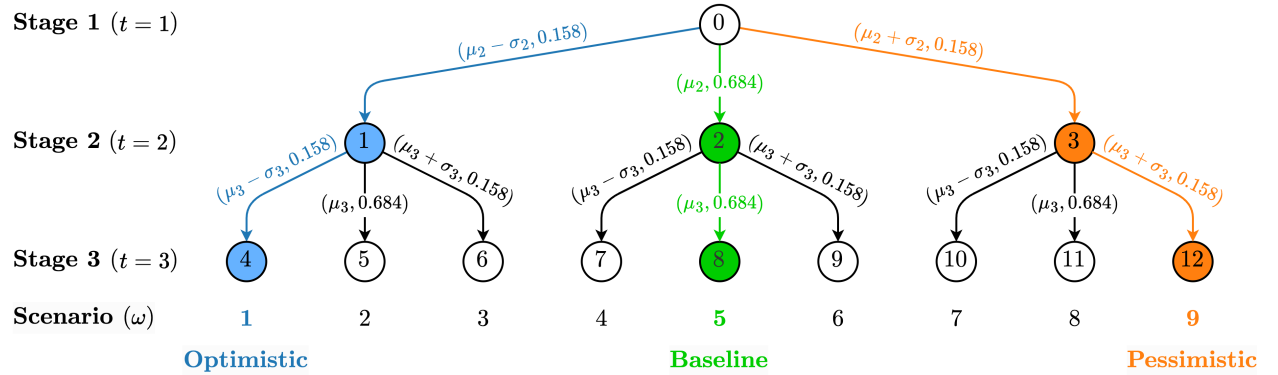
Within a state, varying attitudes towards vaccination and differing vaccination rates significantly impact disease transmission and the resulting need for healthcare resources. We capture variations in VH over time and space via a scenario tree that we describe next.

Scenario tree: Scenario trees provide a systematic approach to represent uncertainty that is suitable for quantitative models. They provide likely scenarios of the future with associated probabilities.

Each scenario ω ($\omega \in \Omega$) represents the changes of VH for a specific population group, over time. We derive temporal changes in VH from the historical data provided by the CTIS. We fit a distribution to the rate of change of VH. Numerical analysis shows that the (monthly) rate of change of VH is normally distributed. The corresponding mean (μ_t) and standard deviation (σ_t) change from one period (month) to the next (see Figure 12). To construct a decision tree of manageable size, we approximate the normal distribution with a discrete triangular distribution that assumes the values μ_t , $\mu_t - \sigma_t$, $\mu_t + \sigma_t$ with probabilities of 0.158, 0.684, and 0.158, respectively.

Figure 2 presents the scenario tree for a problem with $T = 3$ stages. The resulting scenario tree has $3^2 = 9$ unique scenarios. Let p_ω denote the probability associated with each of these scenarios. The tree showcases a baseline (green path), an optimistic (blue path), and a pessimistic (orange path) scenario. In the optimistic scenario, the VH changes by $\mu_t - \sigma_t$ in each stage. In the pessimistic scenario, the VH changes by $\mu_t + \sigma_t$ at each stage. In the baseline scenario, the VH changes by μ_t at each stage. Consequently, the probability associated with the pessimistic and optimistic scenarios is $0.158^2 = 0.024$. The probability associated with the baseline scenarios is $0.684^2 = 0.468$.

Figure 2: A scenario tree illustrating three stages, with each stage branching into three paths, resulting in nine unique scenarios. Branch annotations denote the rate of change and corresponding probabilities.

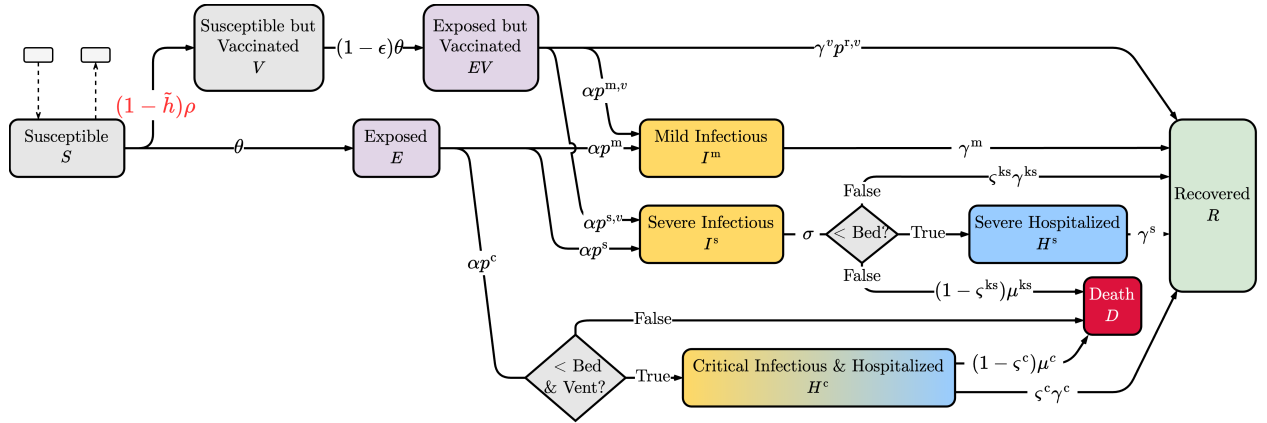


3.2 A compartmental model of COVID-19

The SEIR model divides the population into four groups (compartments): Susceptible (S), Exposed (E), Infectious (I), and Recovered (R). The model captures the transition of individuals through these compartments over time. It also accounts for the latency period before an individual becomes infectious, which is important in modeling the spread of diseases such as COVID-19. In a previous study, our team extended this model to address the specific complexities of COVID-19, such as vaccine availability, VH, and the scarcity of critical healthcare resources in the spread of the disease [Bui et al., 2024]. For the convenience of the reader, we summarize the model in the following paragraphs.

A schematic representation of the proposed susceptible-vaccinated-exposed-infectious-hospitalized-recovered (SVEIHR) model is shown in Figure 3. In this model, susceptible individuals can be exposed or opt to vaccinate, moving forward to the vaccinated compartment (V). The size of compartment V is dictated by ρ , representing the maximum vaccination rate achievable in the absence of VH. The willingness of people to get vaccinated is represented by $(1 - \tilde{h})$, where, \tilde{h} is a stochastic parameter that represents the proportion of the population reluctant to vaccinate. Furthermore, the model considers that vaccination does not confer absolute immunity; therefore, vaccinated individuals can progress to an Exposed but Vaccinated compartment (EV), with a probability determined by vaccine efficacy, ϵ .

Figure 3: SVEIHR: COVID-19 compartmental model that incorporates vaccination dynamics, VH, and healthcare resource constraints.



The model captures different postexposure health trajectories based on incubation rates α and the severity of the disease. Individuals progress to Mild (I^m), Severe (I^s), or Critical Condition (H^c) compartments with probabilities p^m , p^s , and p^c , respectively. Vaccinated individuals are less likely to experience severe/critical health outcomes; thus, several infected individuals are likely to recover and move to the compartment (R).

The model factors the availability of critical healthcare resources, such as hospital beds (**Bed**) and ventilators (**Vent**), in determining patients' health outcomes. Refer to the example presented in Appendix A for a demonstration of the impact of the number of beds and ventilators on the model outcomes. Recovery (γ) and mortality (μ) rates vary depending on the severity of the disease and the availability of healthcare resources. The model accounts for the transition of critically ill patients to the compartment (D) when ventilators are unavailable, emphasizing the dire consequences of resource limitations during a pandemic.

3.3 A compartmental multi-stage stochastic optimization model

This section outlines the formulation of the proposed multi-stage stochastic program (MSP) model. The model determines an optimal sequence of decisions related to ventilator allocation across various regions over time. The MSP minimizes the total number of deaths by dynamically adjusting the distribution of healthcare resources in response to changing VH rates and state transitions within the SVEIHR model. Resource allocation decisions take into account not just immediate health outcomes, but also the need for equitable access to care. By integrating the compartmental model with the MSP model, we now better understand how VH and disease dynamics affects healthcare systems, and use this information to optimize the allocation of ventilators. We refer to this proposed model as the compartmental MSP model. For a detailed description of the model notations used, please see Appendix C.

Model assumptions: Our model operates on three primary sets of assumptions that are critical to its structure and function:

Assumption 1: Uncertainty in vaccine hesitancy (VH): The model considers three potential outcomes of VH in each decision stage. Let h_{t-1} represent the proportion of the population reluctant to vaccinate in period $t - 1$. Then, in period t , the proportion of the population reluctant to vaccinate for the optimistic, expected, and pessimistic scenarios are $h_{t-1}(1 + \mu_t - \sigma_t)$; $h_{t-1}(1 + \mu_t)$; and $h_{t-1}(1 + \mu_t + \sigma_t)$. Each of these outcomes is associated with a fixed probability that does not change over the course of the study. These probabilities remain constant and unaffected by changing decisions. We note that decision makers can customize these outcomes (number of outcomes and values) based on available data.

Assumption 2: Disease dynamics: Since SVEIHR is a compartmental epidemiological model, the following assumptions of SEIR model apply. (i) Every individual in a population is equally likely to interact with others. As a result, disease progression and transitions between compartments are consistent throughout the population. However, it should be noted that in a real-world setting, elements such as social networks and age demographics can significantly influence disease transmission patterns. (ii) The size of the total population does not change due to natural births, non-COVID-19-related deaths, or migration. Since the time frame considered in our study spans several months, recovered individuals are assumed to have full and lasting immunity to the disease. (iii) Infection, recovery, and exposure rates are assumed to be deterministic. However, we recognize that in practice, they can fluctuate for many reasons, from policy interventions and demographic differences to viral mutations.

Assumption 3: Healthcare system: The available healthcare resources (i.e., beds, ventilators) are only used to treat COVID-19 patients. Furthermore, our proposed MSP model does not account for potential reallocations of healthcare resources.

Mathematical model formulation: Classical SIR are continuous-time models. However, several researchers propose discrete-time approximations of these models that are easier to solve [Wacker and Schlüter, 2020]. These studies show that many of the desired properties of the time-continuous SIR models remain valid in the time-discrete approximations. We use a discrete-time model to mimic the dynamic changes in the size of compartments of the SVEIHR model over time. Let \mathcal{T} represent the set of time periods in the planning horizon. Let \mathcal{J} represent the set of decision periods (stages). Note that, between every two consecutive decision periods, there are several time periods, thus $\mathcal{J} \subset \mathcal{T}$. We denote by \mathcal{R} the set of regions studied. We distinguish between a decision stage j and a time period t to keep the discrete approximation of the SEIR model effective, ensuring short time intervals between transitions, while avoiding too many decision stages for the MSP model.

In a decision period (stage), we determine the allocation of ventilators. Our decision variables are $x_{\omega,j,r}$, which represent the number of ventilators assigned to the region $r \in \mathcal{R}$ at the beginning of period $j \in \mathcal{J}$ in scenario $\omega \in \Omega$. Let $\mathcal{X}_{\omega,t,r}$ represent the cumulative number of ventilators allocated to region r by time t .

The decisions made affect the state variables, which are the number of susceptible individuals who are unvaccinated ($S_{\omega,t,r}$) and vaccinated ($V_{\omega,t,r}$); the number of exposed individuals who are unvaccinated ($E_{\omega,t,r}$) and vaccinated ($EV_{\omega,t,r}$); the number of infectious individuals with mild ($I_{\omega,t,r}^m$) and severe ($I_{\omega,t,r}^s$) symptoms; the number of hospitalized individuals in severe ($H_{\omega,t,r}^s$) and in critical ($H_{\omega,t,r}^c$) condition; the number of individuals admitted to a hospital and in severe ($\mathcal{A}_{\omega,t,r}^s$) or critical ($\mathcal{A}_{\omega,t,r}^c$) condition; the number of individuals in severe ($\mathcal{K}_{\omega,t,r}^s$) and critical ($\mathcal{K}_{\omega,t,r}^c$) condition not admitted to the hospital due to capacity constraints; the number of recovered individuals ($R_{\omega,t,r}$); and the number of deaths ($D_{\omega,t,r}$). Let $\mathcal{L} = \{S, V, E, EV, I^m, I^s, H^s, H^c, R, D\}$ represent the set of our state variables.

Next, we provide detailed descriptions of the objective function and constraints of the proposed compartmental MSP.

Objective function: The objective is to minimize the total expected number of deaths across regions during the planning horizon.

$$\mathcal{Z} = \min \sum_{r \in \mathcal{R}} \sum_{\omega \in \Omega} p_{\omega} D_{\omega,|\mathcal{T}|,r} \quad (1)$$

Constraints: We organize our constraints into five groups ($G1, G2, \dots, G5$), each tailored to fulfill a specific function. This structure enhances the model's clarity and highlights the essential contribution of each constraint category to the model's objective.

($G1$): *SVEIHR compartmental model:* This group of constraints captures the dynamic changes of state variables over time. We begin by initializing the state variables $\ell \in \mathcal{L}$ at $t = 0$. Let $\pi_{\ell,r}$ represent the corresponding initial values.

$$\ell_{\omega,0,r} = \pi_{\ell,r} \quad \forall \ell \in \mathcal{L}, r \in \mathcal{R}, \omega \in \Omega \quad (2)$$

Constraints (3)-(12) describe the transition of the population between different compartments of the epidemiological model over time (as illustrated in Figure 3). Constraint (3) updates the size of the susceptible population in com-

partment **S**. To determine the size of **S** at the end of period $t + 1$, we update the size of **S** at the end of period t by subtracting the number of individuals exposed, vaccinated and subtracting (adding) those who immigrated (emigrated) to the region from (to) other regions considered in the analysis. In Appendix F, we provide descriptions of the effects of migration in our model. Constraint (4) updates the size of the vaccinated population, compartment **V**. To determine the size of **V** at the end of the period $t + 1$, we update the size of **V** at the end of period t by subtracting the number of individuals exposed and adding the number of individuals vaccinated. The efficacy rate of the vaccine, ϵ , affects the size of this compartment. Constraint (5) updates the size of the unvaccinated population who were exposed, compartment **E**. To determine the size of **E** at the end of period $t + 1$, we update the size of **E** at the end of period t subtracting the number of individuals exposed who became infected, and by adding the number of individuals exposed during period $t + 1$. Constraint (6) updates the size of the vaccinated population who are exposed, compartment **EV**. This constraint updates the size of **EV** by taking a similar approach to (5). The difference between constraints (5) and (6) is that vaccinated individuals can recover after exposure and do not become critically ill. Constraints (7) and (8) update the size of compartments **I^m** and **I^c**, respectively. To determine the size of compartment **I^m** at the end of $t + 1$, constraint (7) considers new infections, and recoveries. To determine the size of compartment **I^s** at the end of $t + 1$, constraint (8) considers new infections, recoveries, deaths and transitions to the hospitalization compartment. Constraints (9) and (10) update the size of compartments **H^s** and **H^c**. To determine the number of severely hospitalized individuals (the size of compartment **H^s**) at the end of period $t + 1$, constraint (9) considers new admissions, recoveries, and deaths. To determine the number of critically hospitalized individuals (the size of compartment **H^c**) at the end of period $t + 1$, constraint (10) also considers new admissions, recoveries, and deaths. Constraint (11) determines the number of recovered individuals (the size of the compartment **R**) at the end of the period $t + 1$ by aggregating the number of those recovered from various compartments (of infected and hospitalized individuals), each with specific recovery rates. Lastly, the constraint (12) determines the size of the compartment **D**. It compiles the death toll within the region, including deaths from the inability to hospitalize individuals in severe and critical conditions, and deaths among individuals in critical conditions, adjusting to their respective mortality rates.

Constraints (3)-(12) are for all $t \in \{1, \dots, |\mathcal{T}| - 1\}$, $r \in \mathcal{R}$, $\omega \in \Omega$:

$$S_{\omega,t+1,r} = S_{\omega,t,r} - \theta_{\omega,t,r} S_{\omega,t,r} - \rho_r(1 - h_{\omega,t,r}) S_{\omega,t,r} + \sum_{r' \in \mathcal{R}} \nu_{r' \rightarrow r} S_{\omega,t,r'} - \sum_{r' \in \mathcal{R}} \nu_{r \rightarrow r'} S_{\omega,t,r} \quad (3)$$

$$V_{\omega,t+1,r} = V_{\omega,t,r} + \rho_r(1 - h_{\omega,t,r}) S_{\omega,t,r} - (1 - \epsilon) \theta_{\omega,t,r} V_{\omega,t,r} \quad (4)$$

$$E_{\omega,t+1,r} = E_{\omega,t,r} + \theta_{\omega,t,r} S_{\omega,t,r} - \alpha_r E_{\omega,t,r} \quad (5)$$

$$EV_{\omega,t+1,r} = EV_{\omega,t,r} + (1 - \epsilon) \theta_{\omega,t,r} V_{\omega,t,r} - (\alpha_r(p_r^{m,v} + p_r^{s,v}) + \gamma_r^v p_r^{r,v}) EV_{\omega,t,r} \quad (6)$$

$$I_{\omega,t+1,r}^m = I_{\omega,t,r}^m + \alpha_r p_r^m E_{\omega,t,r} + \alpha_r p_r^{m,v} EV_{\omega,t,r} - \gamma_r^m I_{\omega,t,r}^m \quad (7)$$

$$I_{\omega,t+1,r}^s = I_{\omega,t,r}^s + \alpha_r p_r^s E_{\omega,t,r} + \alpha_r p_r^{s,v} EV_{\omega,t,r} - \sigma_r I_{\omega,t,r}^s \quad (8)$$

$$H_{\omega,t+1,r}^s = H_{\omega,t,r}^s + \mathcal{A}_{\omega,t,r}^s - \gamma_r^s H_{\omega,t,r}^s \quad (9)$$

$$H_{\omega,t+1,r}^c = H_{\omega,t,r}^c + \mathcal{A}_{\omega,t,r}^c - (1 - \zeta_r^c) \mu_r^c H_{\omega,t,r}^c - \zeta_r^c \gamma_r^c H_{\omega,t,r}^c \quad (10)$$

$$R_{\omega,t+1,r} = R_{\omega,t,r} + \gamma_r^v p_r^{r,v} EV_{\omega,t,r} + \gamma_r^m I_{\omega,t,r}^m + \gamma_r^s H_{\omega,t,r}^s + \zeta_r^{ks} \gamma_r^{ks} \mathcal{K}_{\omega,t,r}^s + \zeta_r^c \gamma_r^c H_{\omega,t,r}^c \quad (11)$$

$$D_{\omega,t+1,r} = D_{\omega,t,r} + (1 - \zeta_r^{ks}) \mu_r^{ks} \mathcal{K}_{\omega,t,r}^s + (1 - \zeta_r^c) \mu_r^c H_{\omega,t,r}^c + \mathcal{K}_{\omega,t,r}^c \quad (12)$$

(G2) *Resource capacity constraints*: Constraints (13) to (15) determine the values of the decision variables. The initial number of ventilators in hospitals is limited. Consider that Δ_j is the number of new ventilators available for allocation in period (stage) $j \in \mathcal{J}$. Constraints (13) determine the allocation of these ventilators to hospitals in different regions. Constraints (14) determine the total number of ventilators available in region r at period j . Since the number of time periods between every two consecutive decision periods is greater than one, we ensure (via constraints (15)) that the total number of available ventilators does not change until the next decision period.

$$\sum_{r \in \mathcal{R}} x_{\omega,j,r} \leq \Delta_j \quad \forall j \in \mathcal{J}, \omega \in \Omega, \quad (13)$$

$$\mathcal{X}_{\omega,j,r} = \mathcal{X}_{\omega,j-1,r} + x_{\omega,j,r} \quad \forall j \in \mathcal{J}, r \in \mathcal{R}, \omega \in \Omega, \quad (14)$$

$$\mathcal{X}_{\omega,t,r} = \mathcal{X}_{\omega,t-1,r} \quad \forall t \in \mathcal{T} \setminus \mathcal{J}, r \in \mathcal{R}, \omega \in \Omega. \quad (15)$$

Constraint (16) connects the decision variables with the state variables. This constraint determines the number of critically ill patients admitted to a hospital, $\mathcal{A}_{\omega,t,r}^c$. This number depends on the demand for critical care, the number of ventilators available, and the number of beds available.

Constraint (17) determines the number of severely ill patients admitted to a hospital, $\mathcal{A}_{\omega,t,r}^s$. This number depends on the demand for care and beds available after the admission of patients in critical condition. In Appendix D we detail the linearization of “min” functions in constraints (16) and (17). The restrictions (18) and (19) determine the number of patients with severe and critical conditions who were not admitted to a hospital due to limited resources. Constraints (16) to (19) are for all $t \in \mathcal{T}, r \in \mathcal{R}, \omega \in \Omega$.

$$\mathcal{A}_{\omega,t,r}^c = \min \left\{ \alpha_r p_r^c E_{\omega,t,r}, \mathcal{X}_{\omega,t,r} - H_{\omega,t,r}^c, b_r - H_{\omega,t,r}^c - H_{\omega,t,r}^s \right\} \quad (16)$$

$$\mathcal{A}_{\omega,t,r}^s = \min \left\{ \sigma I_{\omega,t,r}^s, b_r - H_{\omega,t,r}^c - H_{\omega,t,r}^s - \mathcal{A}_{\omega,t,r}^c \right\} \quad (17)$$

$$\mathcal{K}_{\omega,t,r}^c = \alpha_r p_r^c E_{\omega,t,r} - \mathcal{A}_{\omega,t,r}^c \quad (18)$$

$$\mathcal{K}_{\omega,t,r}^s = \sigma I_{\omega,t,r}^s - \mathcal{A}_{\omega,t,r}^s \quad (19)$$

(G3:) *Resource allocation constraints:* Equity in healthcare resource distribution, especially during emergencies, is vital for public health policy. Defining and measuring equity in public health decisions is a complex task with no widely accepted standard. We present several approaches used by the literature to ensure fair allocation of healthcare resources (see our discussion of (20)-(22)). Each constraint, when applied individually, offers a distinct approach to resource allocation. Constraint (20), adapted from [Yin and Buyuktahtakin, 2021a], uses information about the proportion of the expected critically ill individuals in a region (the first term in this constraint) and the corresponding population proportion of the region (the second term in this constraint) to allocate ventilators. It uses an equity threshold parameter, denoted by $k \in (0, 1]$, to gauge need-based equity in resource allocation. As k approaches zero, equity in resource allocation is enforced. As the value of k approaches one, the equity requirements become less stringent. In Appendix D, you will find our approach to linearizing this constraint.

$$\left| \frac{\sum_{t \in \mathcal{T}} \sum_{\omega \in \Omega} p_{\omega} H_{\omega,t,r}^c}{\sum_{t \in \mathcal{T}} \sum_{r' \in \mathcal{R}} \sum_{\omega \in \Omega} p_{\omega} H_{\omega,t,r'}^c} - \frac{n_r}{\sum_{r' \in \mathcal{R}} n_{r'}} \right| \leq k \quad (20)$$

The restrictions (21) present a variation in the population-proportional method for the allocation of resources [Dangfield et al., 2019, World Health Organization, 2020]. We include an equity threshold parameter ζ . This constraint ensures that each region receives ventilators in proportion to its share of the total population, with ζ providing adjustable scaling to fine-tune how strictly the allocation of resources follows population size. For $\zeta = 1$, the additional ventilators available for use during period j , denoted as Δ_j , are distributed according to the population size of each region. As ζ decreases, this constraint relaxes, and the equity requirements become less stringent.

$$\sum_{\omega \in \Omega} p_{\omega} x_{\omega,j,r} \geq \left(\frac{n_r}{\sum_{r' \in \mathcal{R}} n_{r'}} \right) \zeta \Delta_j, \quad \forall j \in \mathcal{J}, r \in \mathcal{R}. \quad (21)$$

Both constraints (20) and (21), focus on ensuring an equitable distribution of critical resources. One of the constraints uses a need-based approach, and the other population-based approach to resource allocation.

Constraints (22) ensure that ventilators are distributed equally, ignoring differences in population size or the specific needs of each region. As a result, the same number of ventilators is allocated to every region.

$$\sum_{\omega \in \Omega} p_{\omega} x_{\omega,j,r} \geq \left\lfloor \frac{\Delta_j}{|\mathcal{R}|} \right\rfloor, \quad \forall j \in \mathcal{J}, r \in \mathcal{R}. \quad (22)$$

Notice that we solve the compartmental MSP model with either constraints (20), or (21), or (22) to enforce equity or equality in resource allocation. We also solve the compartmental MSP model without constraints (20), (21), and (22) to demonstrate the effects of a utilitarian approach that aims to minimize the overall cost of resource allocation.

(G4) *Non-anticipativity constraints (NACs):* These constraints ensure that decisions made at a given time (decision stage) are based solely on the information available up to that point. This prevents the use of future, yet unknown, information in decision making. Specifically, constraints (23) ensure that decisions that share an identical scenario path

Table 1: Healthcare capacity by region in Arkansas.

Region	# Counties	Population (Ratio)	Licensed Beds	ICU Beds
R1	18	394,446 (14.45%)	1,405	77
R2	14	1,551,512 (56.84%)	9,357	566
R3	13	171,946 (6.30%)	490	18
R4	30	611,686 (22.41%)	2,032	105
Total	75	2,729,590	13,284	766

up to time j must be consistent and identical across shared paths. In (23), $\mathcal{S}_{\omega,j,r}$ represents the set of scenarios that are indistinguishable from ω at time t . In Appendix E, we provide an example that demonstrates the implementation of these constraints.

$$x_{\omega,j,r} - x_{\omega',j,r} = 0, \quad \forall \omega \in \Omega, \omega' \in \mathcal{S}_{\omega,j,r}, j \in \mathcal{J}, r \in \mathcal{R}. \quad (23)$$

(G5) *Other constraints:* Constraints (24) restrict the decision variables to be non-negative integers. Constraints (25) and (26) restrict the state variables to be nonnegative. The following constraints are also for all $\omega \in \Omega, r \in \mathcal{R}$.

$$x_{\omega,j,r} \in \mathbb{Z}_{\geq 0} \quad \forall j \in \mathcal{J}, \quad (24)$$

$$\ell_{\omega,t,r} \geq 0 \quad \forall \ell \in \mathcal{L}, t \in \mathcal{T}, \quad (25)$$

$$\mathcal{A}_{\omega,t,r}^s, \mathcal{A}_{\omega,t,r}^c, \mathcal{K}_{\omega,t,r}^s, \mathcal{K}_{\omega,t,r}^c \geq 0 \quad \forall t \in \mathcal{T}. \quad (26)$$

4 Data Collection and Model Verification and Validation

To validate the compartmental MSP model, we developed a case study using county-level data from Arkansas during January to May 2021. During this period of the COVID-19 pandemic, vaccines were available to the public. Next, we discuss our data collection, data processing, and our approach to model validation and verification. The SVEIHR and MSP compartmental models presented in Section 3 are modeled using Python 3.10. The optimization model in Section 3.3 is solved using the DOcplex API from CPLEX version 22.1.1. We performed our computational analysis on a system equipped with a 32-core CPU and 192 GB of RAM.

4.1 Data collection and processing

Data collection: We collect data about county-level vaccination uptake from January to May 2021 from the CDC [2021], and data about VH from the CTIS dataset [Salomon et al., 2021]. Data on healthcare resources come from the CovidCareMap [2020] project. Data are organized by facility, county, referral region, and state. Table 1 summarizes the data for Arkansas.

Figure 4(a) presents the county-level distribution of hospitals and licensed beds in Arkansas at the beginning of the COVID-19 pandemic. Figure 4(b) illustrates the relationship between population size and the number of licensed beds in each county. We cluster counties of Arkansas into four regions based on their VH. Below, we provide details of our clustering approach. Figure 4(c) summarizes the total number of licensed beds and intensive care unit (ICU) beds in each region. We assume that each ICU bed has a ventilator. The results of these figures emphasize the variations in healthcare capacity across the state.

Clustering of the data: In an effort to reduce the size of the decision tree of the MSP model, we cluster counties of Arkansas into four regions. The counties are clustered according to their VH similarity. We measure similarity using the Euclidean distance between county-level VH time series data. We use the SciPy Python dendrogram tool to visualize the clustering of counties that belong to the same region (Figure 5(a)) [Virtanen et al., 2020]. We use as a threshold a distance of 0.4 and identify four distinct regions. Figures 5(b)-(e) illustrate VH trends within each region. Each thin line represents the VH of a county, and the dotted line represents the average VH of that region. In particular, Region 3, marked red, starts with the highest VH and, despite the declining trend, remains the highest throughout the study period. In contrast, Region 2, marked green, begins with a VH of 0.39, which then drops dramatically, ending as the region with the lowest VH. Figure 5(f) maps the regions geographically, highlighting that Arkansas's major cities, Fayetteville, Fort Smith, and Little Rock, are in Region 2, which has the lowest VH.

Figure 4: (a) County-level distribution of licensed hospital beds in Arkansas. (b) Relationship between population size and number of licensed hospital beds by county. (c) The total number of licensed and ICU beds, aggregated by region of study.

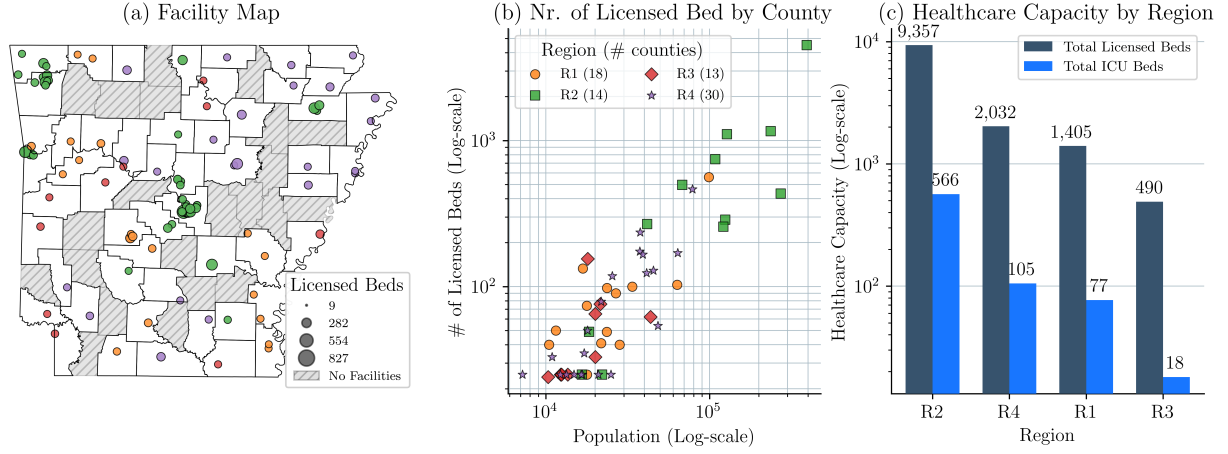
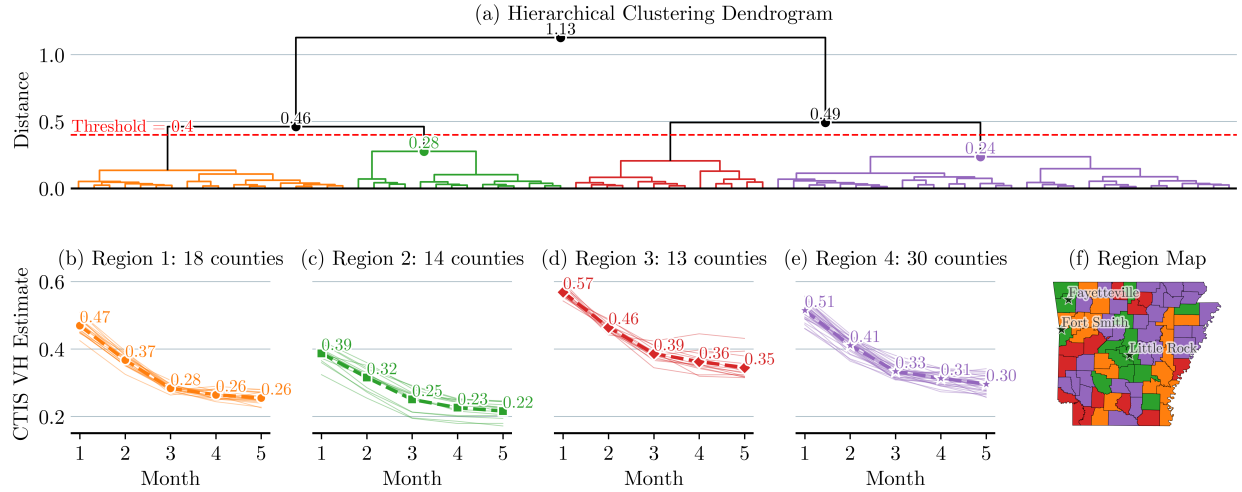


Figure 5: (a) Hierarchical clustering of CTIS VH data for counties in Arkansas. (b)-(e) Region-specific VH trends over five months (January to May 2021). (f) Spatial distribution of the four regions.



Other data processing: Our model employs the parameter Δ_j to indicate the number of ventilators available for distribution among different regions at the start of each decision period, j . The COVID-19 pandemic significantly increased the demand for ventilators, a critical medical device that saved many lives. In response, under Defense Production Act (DPA), various manufacturers, including auto manufacturers, quickly began to increase the production of ventilators or repurpose their facilities for this task [Albergetti and Siddiqui, 2020]. For example, General Motors (GM) was contracted to supply 30,000 medical ventilators for the national stockpile [Massey and Cole, 2020]. In April 2020, AdvaMed reported that its member companies were ramping up production from an average of 2,000 to 3,000 ventilators per week to an expected 5,000 to 7,000 per week. This was a notable increase from the 700 ventilators they produced weekly for the U.S. market in 2019 AdvaMed [2020]. Due to the lack of real-world data related to the additional ventilators allocated to Arkansas after the enactment of DPA, we use the following approach to generate these data.

We use equations (27) to (29) to determine Δ_j . Let p represent the initial stockpile of ventilators in Arkansas prior to enactment of DPA, and let \bar{p} represent an upper bound on the total number of available ventilators. Let p_j represent the additional ventilators made available in period j .

$$\Delta_1 = \underline{p} \quad (27)$$

$$\Delta_j = \Delta_{j-1} + p_j \quad \forall j \in \mathcal{J} \setminus \{1\} \quad (28)$$

$$\Delta_j \leq \bar{p} \quad \forall j \in \mathcal{J} \quad (29)$$

We begin with an initial stockpile (\underline{p}) of 100 ventilators. In each subsequent time period, we increase the number of ventilators (p_j) by 50. As a result, the number of ventilators available for distribution in Arkansas follows this pattern: $\Delta_1 = 100$, $\Delta_5 = 150$, $\Delta_9 = 200$, $\Delta_{13} = 250$, and $\Delta_{17} = 300$.

Please refer to tables in Appendix G for a complete list of the parameter values used in our MSP compartmental model. The table also presents the tuned parameters, which are outcomes of the model calibration process detailed in Section 4.2.

4.2 Calibration of the compartmental model

The calibration of SVEIHR focuses on fine-tuning the model parameters to ensure that it accurately represents the dynamics of disease progression in each region of study. We collected data from COVID-19 Open Data [Wahltinez et al., 2020]. This dataset provides county-level data. For the purpose of this study, we aggregate county-level data for Arkansas into the four aforementioned regions.

We use data from two critical time periods in the U.S. The first spans 20 weeks, from October 25, 2020 to March 7, 2021. This period includes the peak of the wave of coronavirus infections during the Fall of 2020. We use these data to evaluate SVEIHR’s power in predicting new infections. The second spans 20 weeks, from January 10 to May 23, 2021, and corresponds to the initial stages of vaccine rollout. We use these data to evaluate SVEIHR’s power in predicting vaccinations. These study periods do not coincide with the start of the pandemic. Therefore, we adjust the size of the initial susceptible population to account for individuals who were infected, recovered, or died prior to the start of the study period.

Figure 6 summarizes the results of our model calibration of the baseline scenario. Each plot in this figure presents the actual data and SVEIHR model predictions of the weekly number of infections and vaccination intakes for each region of study. New infections at time t are calculated using this equation: $\alpha(p^m + p^s)E_{t,r} + \alpha(p^{m,v} + p^{s,v})EV_{t,r}$. The cumulative number of vaccinations up to week t is calculated using $\sum_t (1 - h_{t,r})\rho_r S_{t,r}$. We employ the Optuna framework to optimize parameter tuning [Akiba et al., 2019]. Table 2 summarizes the different performance metrics that we use to evaluate the performance of SVEIHR model of the baseline scenario, including root-mean-square error (RMSE), mean absolute error (MAE), and mean absolute percentage error (MAPE). The low value of MAPE highlights the accuracy of SVEIHR in tracking new infections and vaccination trends in each region.

Figure 6: Comparison of predictions from the calibrated SVEIHR model and actual data across four regions for the baseline scenario, illustrating new infections and cumulative vaccinations over time.

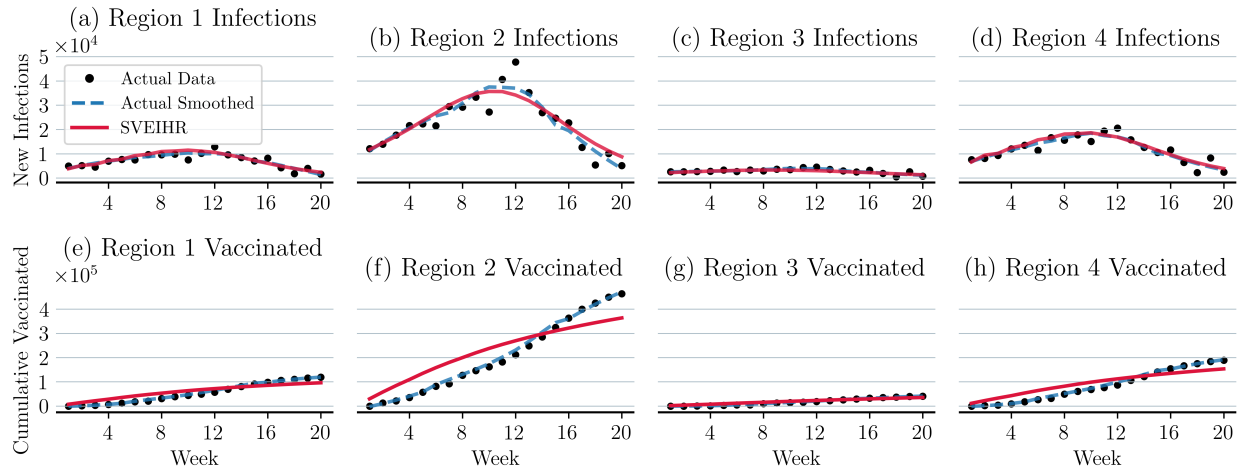


Table 2: Statistical analysis of prediction error from the calibrated SVEIHR model for the baseline scenario.

Region	Infections: Fig. 6(a) - (d)			Vaccinations: Fig. 6 (e)-(h)		
	RMSE	MAE	MAPE	RMSE	MAE	MAPE
R1	705.43	545.28	0.10%	17,094.55	15,883.84	2.00%
R2	2,288.45	1,877.74	0.16%	62,287.10	57,541.79	1.50%
R3	394.94	292.13	0.10%	4,531.79	4,177.05	4.06%
R4	765.10	620.95	0.06%	26,119.66	24,296.23	2.11%

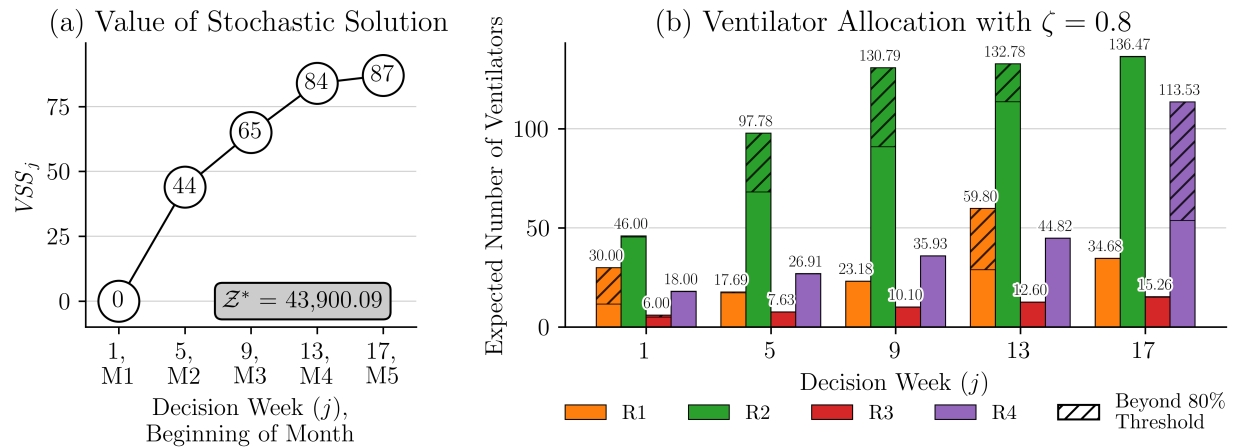
4.3 Value of stochastic solution

The value of stochastic solution (VSS) quantifies the benefit of incorporating uncertainty into decision-making processes by comparing the results of the compartmental MSP with those of its deterministic counterpart. To compute the VSS for each decision stage $j \in \mathcal{J}$, we adopt the methodology proposed by Escudero et al. [2007]. In this method, the expected value (EV) model, which operates on the expected values of uncertain parameters, is used as the deterministic benchmark. Let EEV_j denote the optimal value of the proposed compartmental MSP model when the solution up to the decision period immediately preceding j is fixed to the solution from the deterministic model. Let \mathcal{Z}^* denote the optimal objective function value of the compartmental MSP model. Therefore, VSS at stage j , represented as $VSS_j = EEV_j - \mathcal{Z}^*$, captures the value derived from accommodating uncertainty in the model up to decision stage j .

The evolution of the VSS across the decision stages is illustrated in Figure 7(a). For the model used in this illustration, there are 5 decision stages that correspond to weeks 1, 5, 9, 13, and 17. The results of this figure highlight the benefits derived from the proposed compartmental MSP model. The VSS starts at zero, which is expected since $EEV_1 = \mathcal{Z}^*$. As the model progresses through the stages, the VSS trends upward, reflecting the benefits of incorporating uncertainty into strategic decision making. We notice a decrease in the rate of change in VSS from week 13 to 17. This is mainly because the mean change in VH is lower during these weeks. The results in Figure 12 show that the mean change in VH from week 13 to week 17 ranged from 0.03 to 0.05, which is lower than 0.06-0.09 seen from weeks 9 to 13.

Note that $VSS_j = 87$ in the illustrative example in Figure 7(a) appears to be a rather small number compared to the optimal solution $\mathcal{Z}^* = 43,900$. In this example, a critically ill patient uses a ventilator for three weeks, the recovery rate is 51% and $\bar{p} = 300$. This leads to a total of 1,000 ventilators available for allocation and use over five months, and a maximum of 729 critically ill patients to be saved using these ventilators. Thus, a $VSS_j = 87$ represents 12.21% of this total, which is pretty high and highlights the value of using the compartmental MSP.

Figure 7: (a) Value of stochastic solution of the proposed model. (b) Expected ventilator allocation to different regions.



Note. Compartmental MSP model include constraint (21) with ζ is set to 0.8. The total number of ventilators available in each decision period: $\Delta_1 = 100$, $\Delta_5 = 150$, $\Delta_9 = 200$, $\Delta_{13} = 250$, $\Delta_{17} = 300$.

5 Discussion of the Results

RQ1: *Can we develop an effective resource allocation model of critical resources needed during disease outbreaks?*

To respond to this research question, we develop the compartmental MSP model that facilitates resource allocation decisions under uncertainty. We make three observations: (i) *The compartmental MSP model facilitates capacity allocation decisions given the progression and spread of a disease.* One could also simulate the SVEIHR model for different values of the number of ventilators available during the planning period and for different assignments of these ventilators to regions of study. However, such an approach would be time-consuming. (ii) *The MSP model, rather than its deterministic counterpart, leads to better decision making under uncertainty.* We demonstrate this via our discussion of the VSS in Section 4.3. (iii) *The MSP model facilitates incorporating fairness in capacity allocation decisions.*

Let us demonstrate these observations using the example in Figure 7(b). The figure shows the allocation of ventilators among our four study regions over a 20-week planning period. The decision periods are weeks 1, 5, 9, 13 and 17. In this experiment, we use an equity threshold $\zeta = 0.8$, which enforces that 80% of the ventilators are allocated based on the population size of each region. The remaining 20% of the ventilators are allocated in a way that minimizes the objective function. To help visualize the results, we use a different color for each region. The hatched portions of the bars represent the allocation of the remaining 20% of the ventilators. These results indicate that in the early stages (weeks 5 and 9), the model allocates the additional ventilators to region 2 since this region’s population size and density are the highest. Its population corresponds to 56.84% of the total. Allocating additional ventilators to this region has the greatest impact on reducing the number of deaths. Later in the planning period, additional ventilators are allocated to regions 1 and 4. This is due to an increase in COVID-19 cases and increased vulnerability within these regions. These dynamic adjustments of resource allocation emphasize the model’s ability to respond to changing needs throughout the pandemic, providing an efficient and fair distribution of resources.

These observations highlight the value that the MSP model brings to decision makers during health crises, enabling them to balance between efficiently and equitably allocating scarce critical resources.

RQ2: *What should be effective resource allocation strategies at the start of an outbreak?*

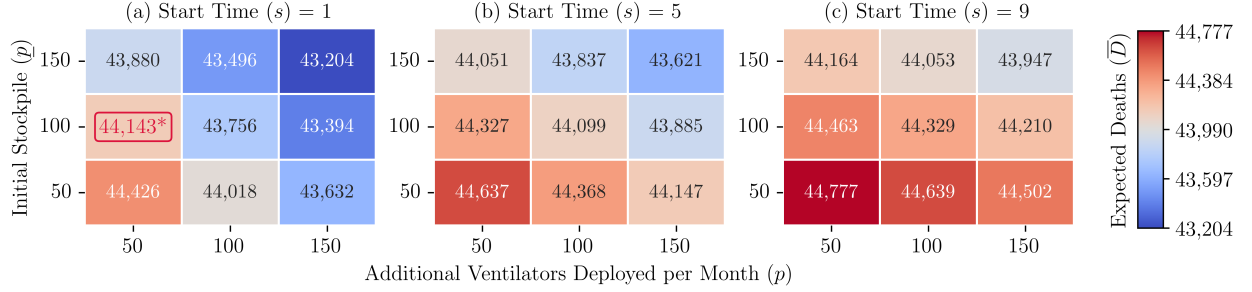
To answer this research question, we designed the following experiment. We create three sets of problems. In each set, the time at which additional ventilators are deployed is different. In set 1, additional ventilators are deployed beginning in period 1. In set 2, that happens in period 5, and in set 3, it happens in period 9 of a 20-week planning period. Each set consists of 9 problems, one for different combinations of the initial stockpile (p) and the number by which we increase the number of ventilators deployed in each period (p_j). These experiments help us understand the impact of the timing and scope of decisions related to increasing the availability of critical resources (such as the timing and scope of the DPA) on the total expected number of deaths. A summary of the results from these experiments is presented in Figure 8. Detailed solution results for a problem from set 1 with $\underline{p} = 100, p_j = 50$, are presented in Figure 7(b).

We make the following observations: (i) *The timing of decisions related to the deployment of critical resources greatly impacts the expected number of deaths.* Based on our experiments, beginning the deployment of ventilators in the 1st rather than in the 9th week of the planning period could lead to an 1.30% average of decrease in the expected number of deaths, which corresponds to 571 individuals. (ii) *The size of the initial stockpile and the number by which we increase the availability of our critical resource every period greatly impact the expected number of deaths.* We develop a simple linear regression model to explore the relationships between the time of deployment of additional ventilators (s), initial stockpile (\underline{p}), the number of additional ventilators deployed (p_j), and expected deaths (\overline{D}). Since in our experiments, we keep p_j constant over time, below, we use p instead. The model is described by:

$$\overline{D} = 44527.66 + 285.41 s - 5.44 \underline{p} - 4.81 p \quad (30)$$

This regression model has an adjusted $R^2 = 0.9477$, which shows that the timing of ventilator deployment, initial stockpile, and the amount by which we increase resource availability explain approximately 94.77% of the variation in the expected number of deaths. Based on our experiments, delaying the start of the deployment of additional ventilators by one month could lead to an average increase in the expected number of deaths by 285.41/month, highlighting the importance of prompt action. Each additional ventilator in the initial stockpile and each additional ventilator deployed lead to a decrease in the expected number of deaths by 5.44 (equivalent to 1.09/month) and 4.81 (0.962/month), respectively, highlighting the importance of maintaining a large stockpile and scalable production responses.

Figure 8: Impact of varying timing of the deployment and the number of new ventilators on the expected death toll.



Note. * The ventilator allocation is shown in Fig. 7.

RQ3: What are the trade-offs between equity, equality, and effectiveness of resource allocation at the onset of a pandemic?

To answer this research question, we designed the following experiment. We create four problems, P1 to P4. The compartmental MSP model without constraints (20), (21) and (22) determines a resource allocation strategy that minimizes the expected number of deaths. This is our first problem (P1), which maximizes efficiency. The compartmental MSP model with constraints (20) focuses on the equitable distribution of resources. As we change the value of the tolerance level $k \in (0, 1]$ from 0 to 1, the equity requirements become less stringent. This is our second problem (P2). The compartmental MSP model with constraints (21) is our third problem (P3), which also focuses on the equitable distribution of resources. As we change the value of the tolerance level $\zeta \in (0, 1)$ from 0 to 1, the equity requirements become rigid. The compartmental MSP model with constraints (22) is our fourth problem (P4), which focuses on the equal distribution of resources. The decision periods and the availability of resources are similar to the experiment described in **RQ1**.

We make the following observations: (i) *Strategies that focus on equality underperform those that focus on efficiency and equity.* Figure 9(e) presents the total expected number of deaths as the value of k changes from 10^{-3} to 1 (P2), and ζ changes from 0.97 to 0 (P3). Straight lines at 44,594 and 43,900 represent the expected deaths when ventilators are distributed equally (P4) and efficiently (P1), respectively. Based on these results, equal distribution of resources leads to the highest expected number of deaths.

In our experiments, as the value of k increases, the equity restrictions become less stringent, and the expected number of deaths decreases from 44,453 to 43,900, representing a 1.24% decrease. Decreasing ζ makes equity restrictions less stringent, reducing the expected number of deaths from 44,208 to 43,900, which represents a 0.70% decrease. The expected number of deaths is lowest when $k = 1$, or $\zeta = 0$, which represents a model that focuses on efficiency (P1).

(ii) *The price of ensuring equitable allocation of resources changes over time and space. This price is highest during the peak of a disease outbreak and in highly populated regions.* Figures 9(a) - (d) present the expected number of deaths in each region as the value of k increases from 10^{-3} to 1, and the value of ζ decreases from 0.97 to 0. As k increases and as ζ decreases, the equity restrictions become less stringent. These changes affect the regions of study differently. Region 3, which has the smallest population size and the lowest density, benefits the most when equity is enforced (the value of k is close to 10^{-3}). Region 2, which has the largest population size and the highest density, benefits the most when equity is not enforced (the value of k is close to 1). Table 3 summarizes the expected number of deaths for each problem. The table also summarizes the change in the number of deaths for all problems compared to the results of P1.

To evaluate the impact that the timing of resource allocations has on the expected number of deaths, we performed the following experiment. We solve P2 several times by changing the time period over which we enforce the equity constraints (20). Thus, instead of adding for $t \in \mathcal{T}$, we add over $t \in \{\mathcal{T} | t \geq t'\}$, which means that the equity in resource allocation is enforced after t' . Prior to t' , resource allocation is focused on maximizing efficiency. We solve P2 for different values of t' and for different values of k . The results of these experiments are summarized in Figure 10. These results show a decreasing trend in the expected number of deaths as k approaches 1 and t' approaches $|\mathcal{T}|$.

This analysis is important for decision makers considering the appropriate level of equity tolerance that harmonizes both public health objectives and ethical standards. Our analysis provides a data-driven framework for such decisions, emphasizing the necessity of a comprehensive approach that aims to balance the imperative of saving lives and the principles of fairness and justice in resource allocation.

Figure 9: (a)-(d) Expected deaths at different equity levels for each region. (e) Total expected deaths for different resource allocation strategies.

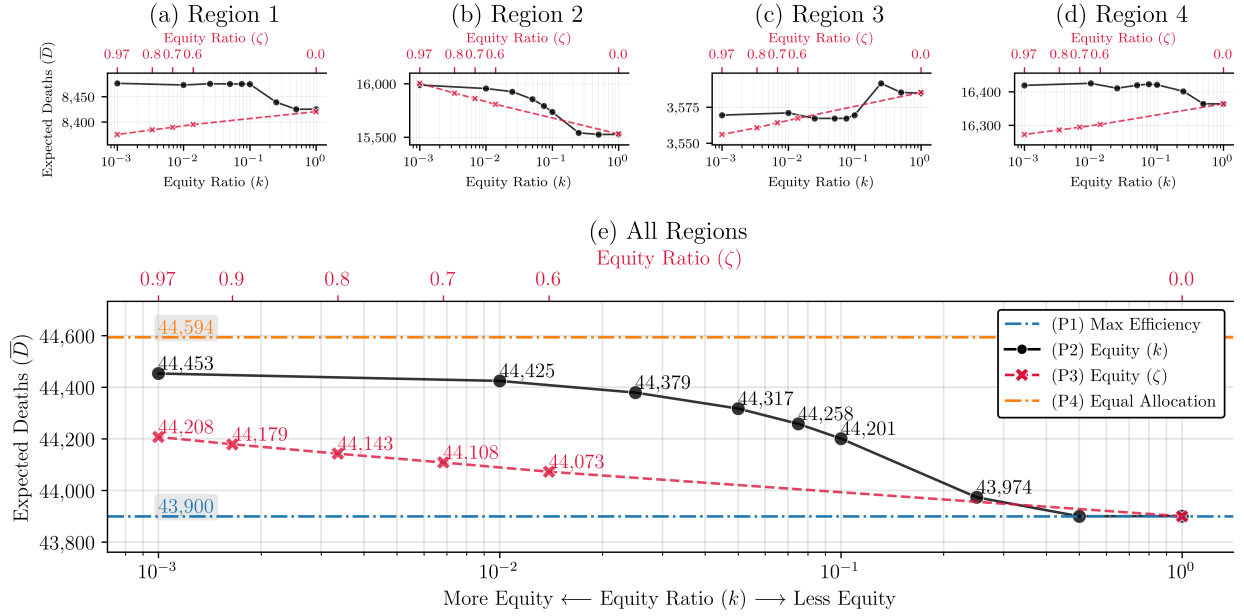
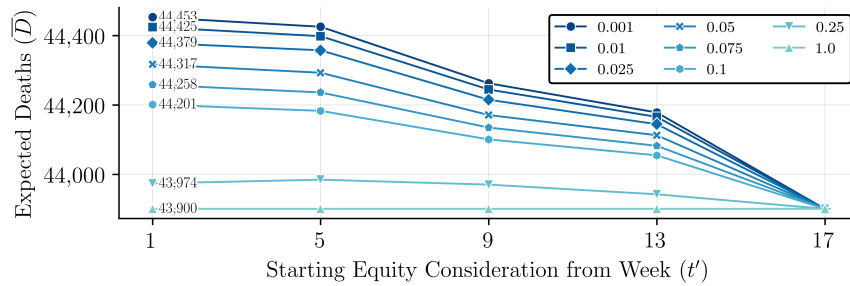


Table 3: Total expected deaths when applying different allocation strategies.

Strategy		Expected Death					Diff from (P1)
		R1	R2	R3	R4	Total	
(P1) Max efficiency		8,427	15,524	3,585	16,364	43,900	—
(P2) Equity (k)	0.001	8,477	15,988	3,569	16,419	44,453	553
	0.05	8,475	15,855	3,567	16,420	44,317	417
	1	8,425	15,527	3,585	16,364	43,900	0
(P3) Equity (ζ)	0.97	8,375	16,004	3,556	16,272	44,208	308
	0.8	8,384	15,912	3,561	16,286	44,143	243
	0.6	8,395	15,808	3,567	16,303	44,073	173
(P4) Equal allocation		8,349	16,480	3,505	16,260	44,594	694

Figure 10: Evaluating the timing of resource allocation decisions on the expected number of deaths.



Note. Summary of results from solving P2 at different time t' .

6 Conclusion and future research directions

Summary of the Proposed Research: This study proposes a modeling framework that integrates a compartmental model within a multi-stage stochastic program (MSP) to tackle the complex challenge of allocating scarce healthcare resources during infectious disease outbreaks. The compartmental model simulates the dynamic changes of vaccine hesitancy (VH) over time and space, improving the ability of MSP to adapt resource allocation strategies to the dynamics of disease spread and changes in population behavior toward vaccines. This compartmental MSP model also allowed us to analyze the price of fairness in resource allocation. Through our numerical analysis, we gain a deeper understanding of the impacts that the deployment time and size of the resource allocation, the effectiveness in managing the spread of the disease, and the price of fairness in resource allocation have on the expected number of deaths. The results of our analysis highlight the importance of advanced planning and preparedness for future outbreaks, effective management of critical resources, and the balance of equity and effectiveness in resource allocation.

Research Contributions: The main contribution of this work is the development of a compartmental MSP model that captures the impact of VH in the effectiveness of allocating critical healthcare resources during a disease outbreak. The results of our numerical analysis show how public behaviors towards the COVID-19 vaccine impacted disease dynamics and the need for healthcare resources.

Our review of the literature showed that there is very limited research on compartmental MSP models. Our proposed data-driven MSP compartmental model fills this gap in the literature and provides a robust framework for planning responses to disease outbreaks. The model supports dynamic decision-making over time and space, taking into account the unpredictable nature of disease spread and resource availability. The model shows how dynamic, evidence-based strategies can enhance public health responses. The model addresses the price of fairness in the allocation of scarce healthcare resources. The model supports effective vaccination strategies and resource allocations that ensure greater immunity and mitigate the impact of outbreaks.

Research Findings: Key observations from our study include: (i) The proposed compartmental MSP model offers a more effective framework for resource allocation than an MSP model, as it captures the impact of disease progression (accounting for varying levels of VH) on the need for critical healthcare resources. (ii) The proposed model supports resource allocation in different regions over time by considering both population size and immediate needs for medical resources, and balancing fairness and efficiency in decision making processes. (iii) The size of the initial stockpile, the timing of deployment of additional resources, and the number of additional resources have a significant impact on the expected number of deaths. Based on our numerical analysis, each unit increase in the initial stockpile and each unit increase of available ventilators could lead to a decrease in the expected number of deaths by 1.09/month and 0.962/month, respectively. Based on our numerical analysis, delaying the deployment of critical resources by a month could increase the expected number of deaths by 285.41/month. (iv) An equal resource allocation strategy results in the highest number of expected deaths (that is, 44,594 over 5 months, assuming that 1,000 become available during this period), while a utilitarian resource allocation results in the smallest (i.e., 43,900 over 5 months). (v) The timing of the implementation of equity in resource allocation greatly impacts health outcomes. Delaying its implementation reduces deaths to levels comparable to those achieved via a utilitarian approach.

Future Research Directions: The model presented in this study can be extended in multiple ways to address other relevant problems related to the allocation of critical healthcare resources. The compartmental MSP models could be extended to capture the interactions between various health interventions (i.e., masking mandates, travel restrictions, school closures, etc.) and the allocation of critical resources under uncertainty. These interventions affect the distribution of VH and the infection rate over time and space. Assume that the VH and infection rate are the uncertain problem parameters considered. In this case, the distribution of random variables is affected “endogenously” by decisions made by the model. MSPs with endogenous uncertainty are more difficult to solve compared to models with exogenous uncertainty.

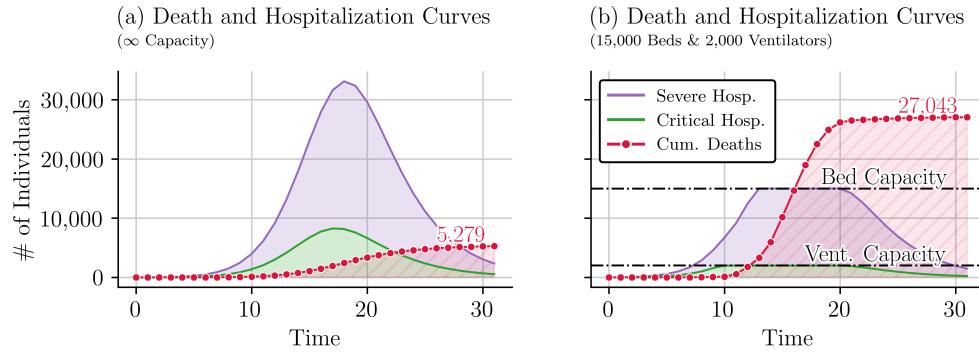
Our proposed model can be extended to support other comparative studies across different regions or demographics to understand the effectiveness of strategies for allocating critical healthcare resources. In addition to the resources considered in our study, the proposed model could be extended to evaluate the impact of allocation strategies for other critical health resources (such as personal protective equipment, testing kits, and hospital beds) on the spread of the disease and the expected number of deaths.

These model extensions provide opportunities to develop novel solution approaches and address relevant healthcare-related problems.

Appendix A Impact of Healthcare Resources on Disease Outcomes

The availability of healthcare resources such as beds and ventilators plays a critical role in managing the outcomes of infectious diseases. We performed two simulations of the SVEIHR model to explore these relationships. The first simulation assumes unlimited healthcare resources, and the second introduces bed and ventilator availability constraints to reflect a real-world scenario with limited resource availability. The outcomes of the first simulation, depicted in Figure 11(a), show a low number of hospitalizations and deaths due to the assumption of infinite resources. However, the results of the second simulation, presented in Figure 11(b), reveal a higher number of deaths due to limited healthcare resources. The increase in the cumulative number of deaths becomes apparent when the number of individuals in critical condition exceeds the number of beds available. The contrast is notable. When the number of beds is unlimited, the expected number of deaths is 5,239, whereas when the number of beds is limited, the model results in 28,507 deaths.

Figure 11: Comparative impact of healthcare resource availability on the SVEIHR model outcomes, illustrating differences in hospitalization and death rates under unlimited and limited resources scenarios.



Appendix B Modeling Uncertainty in Vaccine Hesitancy

Figure 12 shows that the rate of change in vaccine hesitancy fits the Normal Distribution. The corresponding mean and standard deviation changes over time.

Figure 12: (a)-(d) Distribution of the monthly rate of change of vaccine hesitancy for different clusters in the study, with each row representing transitions from the previous month.

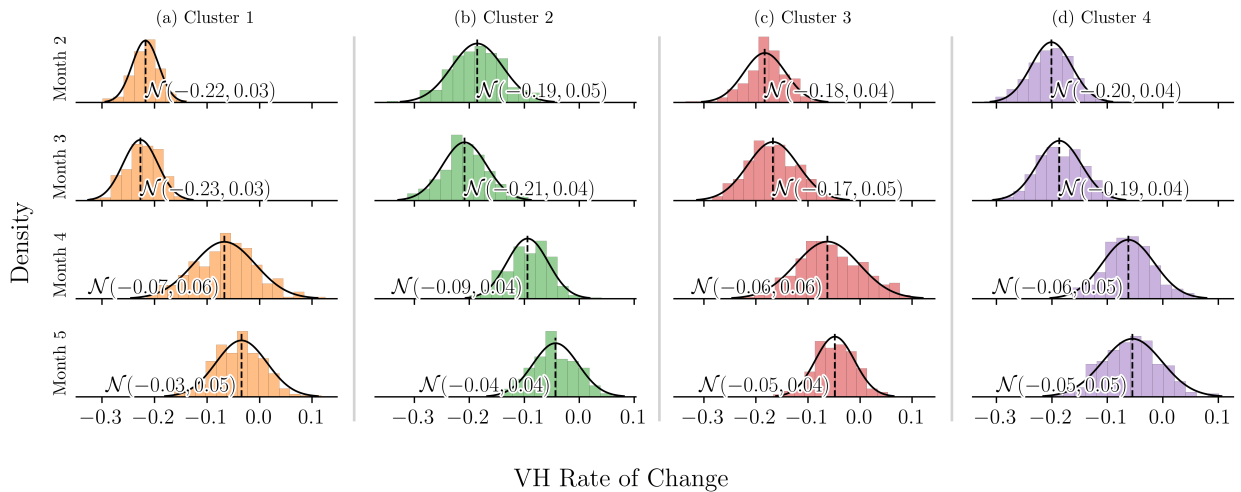


Table 4: Sets and indices in the proposed MSP.

Set	Index	Description
\mathcal{T}	t	Set of time periods.
\mathcal{J}	j	Set of decision time periods, $\mathcal{J} \subset \mathcal{T}$.
\mathcal{R}	r	Set of regions.
Ω	ω	Set of scenarios.
\mathcal{L}	ℓ	Set of state variables after fitting the SVEIHR model with actual data.
$\mathcal{S}_{\omega,j,r}$		Set of scenarios that are indistinguishable with ω at decision stage j .

Table 5: Variables in the proposed MSP.

Variable	Description (for $r \in \mathcal{R}$, at time $t \in \mathcal{T}$, $j \in \mathcal{J}$, and under scenario $\omega \in \Omega$)
$x_{\omega,j,r}^{(1)}$	Ventilators allocated at the start of decision period j .
$\mathcal{X}_{\omega,t,r}$	Cumulative numbers of ventilators at the end of time t .
$S_{\omega,t,r}, V_{\omega,t,r}$	Number of susceptible individuals who are unvaccinated and vaccinated, respectively.
$E_{\omega,t,r}, EV_{\omega,t,r}$	Number of exposed individuals who are unvaccinated and vaccinated, respectively.
$I_{\omega,t,r}^m, I_{\omega,t,r}^s$	Number of infectious individuals with mild and severe symptoms, respectively.
$H_{\omega,t,r}^s, H_{\omega,t,r}^c$	Number of hospitalized individuals with severe and critical conditions, respectively.
$\mathcal{A}_{\omega,t,r}^s, \mathcal{A}_{\omega,t,r}^c$	Number of hospital admissions for severe and critical cases, respectively.
$\mathcal{K}_{\omega,t,r}^s, \mathcal{K}_{\omega,t,r}^c$	Number of severe and critical cases not admitted to the hospital due to capacity constraints.
$R_{\omega,t,r}$	Cumulative number of recovered individuals up to period t .
$D_{\omega,t,r}$	Cumulative number of deaths up to period t .

⁽¹⁾ decision variable

Appendix C Model Notation

Tables 4, 5, and 6 represent the model notations that are used throughout the paper.

Table 6: Parameters in the proposed MSP.

Parameter	Description
$h_{\omega,t,r}$	Vaccine hesitancy rate at region r and time t under scenario ω .
β_r	COVID-19 contact rate in region r . $\theta_{\omega,t,r} = \beta_r S_{\omega,t,r} (I_{\omega,t,r}^m + I_{\omega,t,r}^s) / n_r$.
ρ_r	Maximum vaccination rate in region r .
ϵ	Vaccine efficacy.
α	Incubation rate.
γ_r^m, γ_r^s	Recovery rates for mild and severe cases in region r .
$\gamma_r^{ks}, \gamma_r^c$	Recovery rates for non-hospitalized severe and critical cases in region r .
σ_r	Rate from symptoms to hospitalization in region r .
μ_r^{ks}, μ_r^c	Mortality rates for non-hospitalized severe and hospitalized critical cases in region r .
$\varsigma_r^{ks}, \varsigma_r^c$	Recovery rates for non-hospitalized severe and hospitalized critical cases in the region r .
k	Equity threshold in constraint (20).
ζ	Equity threshold in constraint (21).
$p^m, p^{m,v}, p^s, p^{s,v}$	Transition percentages to mild and severe cases for unvaccinated and vaccinated individuals.
$p^{r,v}$	Recovery rate for vaccinated individuals.
$\pi_{l,r}$	Initial count of individuals in state ℓ (compartment in SVEIHR model) at time $t = 0$ in region r .
n_r	Population size of region r .
b_r	Hospital bed count in region r .
Δ_t	Additional ventilators available to allocate at start of time t .

Appendix D Constraint Linearization

The proposed compartmental MSP model presented in Section 3.3 contains three non-linear constraints. They can be linearized as follows:

We linearize the ‘**min**’ functions in constraints (16) and (17) using the big-M method. To illustrate, let’s consider the linearization of constraint (17). For ease of demonstration, let us declare a few auxiliary variables: $a_1 = \sigma I_{\omega,t,r}^s$ representing the number of severe case admissions and $a_2 = b_r - H_{\omega,t,r}^c - H_{\omega,t,r}^s - \mathcal{A}_{\omega,t,r}^c$ representing the remaining bed capacity after accounting for current hospitalizations.

The original constraint can be written as $\mathcal{A}_{\omega,t,r}^s = \min\{a_1, a_2\}$, indicating that the number of severe cases admitted is the lesser of the demand or the remaining capacity. We use a binary variable ($y_{\omega,t,r}$) and big-M constant (M) to enforce $A \geq \min\{a_1, a_2\}$. The original ‘**min**’ constraint is then replaced by the following system of linear inequalities (17a)-(17d):

$$\mathcal{A}_{\omega,t,r}^s \leq a_1 \quad (17a)$$

$$\mathcal{A}_{\omega,t,r}^s \leq a_2 \quad (17b)$$

$$\mathcal{A}_{\omega,t,r}^s \geq a_1 - M(1 - y_{\omega,t,r}) \quad (17c)$$

$$\mathcal{A}_{\omega,t,r}^s \geq a_2 - My_{\omega,t,r} \quad (17d)$$

Next, we linearize the absolute function in constraint (20) using the following procedure. Again, for demonstration purposes, let us introduce the following auxiliary variables: $a_1 = \sum_{t \in \mathcal{T}} \sum_{\omega \in \Omega} p_{\omega} H_{\omega,t,r}^c$, and $a_2 = \sum_{t \in \mathcal{T}} \sum_{r' \in \mathcal{R}} \sum_{\omega \in \Omega} p_{\omega} H_{\omega,t,r'}^c$. Since $a_2 > 0, \sum_{r' \in \mathcal{R}} n_{r'} > 0$, the original constraint can be written as $\left| \frac{a_1}{a_2} - \frac{n_r}{\sum_{r' \in \mathcal{R}} n_{r'}} \right| \leq k$ and is equivalent to:

$$\begin{aligned} & \begin{cases} \frac{a_1}{a_2} - \frac{n_r}{\sum_{r' \in \mathcal{R}} n_{r'}} \leq k \\ \frac{a_1}{a_2} - \frac{n_r}{\sum_{r' \in \mathcal{R}} n_{r'}} \geq -k \end{cases} \\ \Leftrightarrow & \begin{cases} a_1 \left(\sum_{r' \in \mathcal{R}} n_{r'} \right) - a_2 n_r \leq k a_2 \left(\sum_{r' \in \mathcal{R}} n_{r'} \right) \\ a_1 \left(\sum_{r' \in \mathcal{R}} n_{r'} \right) - a_2 n_r \geq -k a_2 \left(\sum_{r' \in \mathcal{R}} n_{r'} \right) \end{cases} \end{aligned}$$

Constraint (20) can be replaced by the following linear inequalities (20a)-(20b):

$$a_1 \left(\sum_{r' \in \mathcal{R}} n_{r'} \right) - a_2 n_r - k a_2 \left(\sum_{r' \in \mathcal{R}} n_{r'} \right) \leq 0 \quad (20a)$$

$$a_1 \left(\sum_{r' \in \mathcal{R}} n_{r'} \right) - a_2 n_r + k a_2 \left(\sum_{r' \in \mathcal{R}} n_{r'} \right) \geq 0 \quad (20b)$$

Appendix E Illustration of non-anticipativity constraints (NACs)

Figure 13(a) shows a scenario tree with three stages and nine possible scenarios. Figures 13(a) and (b) help the reader understand the implications of the nonanticipativity constraints (NAC). NACs ensure that decisions made at a certain stage are the same across all scenarios that share the same history up to that stage. For example, the root node (stage 1) in Figure 13(a) is colored cyan. This node is common in all scenarios. As such, decisions made in stage 1 affect decisions made along all scenario paths. This is why in Figure 13(b), the nodes in the top layer are all colored cyan. Therefore, the set of scenarios that are indistinguishable from $\omega = 1$ at time $t = 1$ is $\mathcal{S}_{1,1,r} = \{2, 3, \dots, 9\}$. We use the following eight NACs to ensure this: $x_{1,1,r} = x_{2,1,r}$; $x_{1,1,r} = x_{3,1,r}$; \dots ; $x_{1,1,r} = x_{9,1,r}$.

Appendix F Population Flow

We utilized data related to county-to-county migration flows from 2016 to 2020, sourced from [U.S. Census Bureau, 2020]. We estimate the annual movement of individuals between counties in Arkansas. The results are shown in

Figure 13: (a) Illustration of a scenario tree with three stages and nine scenarios, (b) an alternative form to visualize the NACs, which are shown in red.

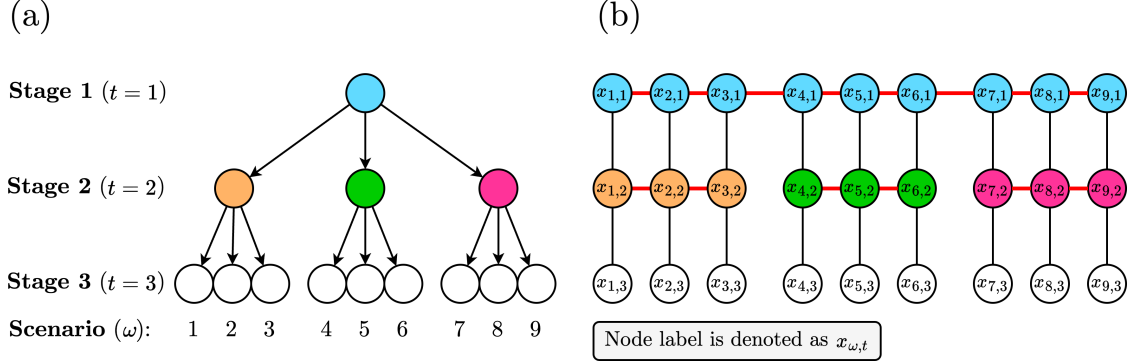
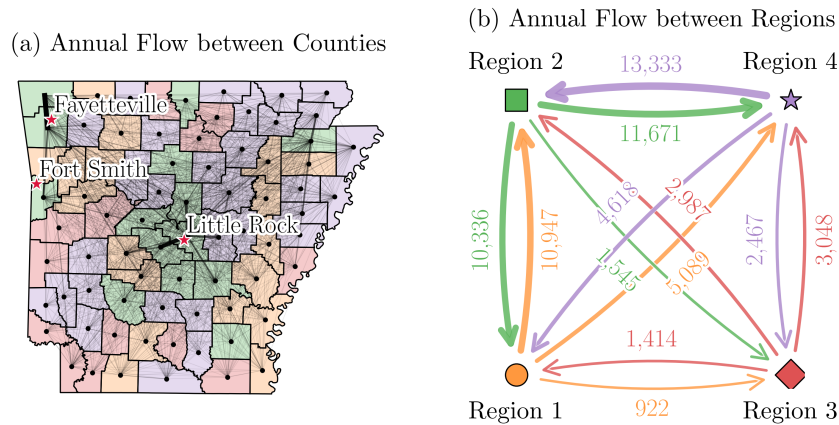


Table 7: Weekly population movement rate between studied regions.

From \ To	R1	R2	R3	R4
R1	-	5.34e-04	4.50e-05	2.48e-04
R2	1.28e-04	-	1.92e-05	1.45e-04
R3	1.58e-04	3.34e-04	-	3.41e-04
R4	1.45e-04	4.19e-04	7.76e-05	-

Figure 14(a). The black dots in this figure represent county centroids and the shaded areas represent the four different regions of study. Major cities like Fayetteville, Fort Smith, and Little Rock are labeled, signifying possible hubs of migration. The simplified flow between regions is depicted in Fig. 14(b). These data are integrated into the compartmental MSP model to update the susceptible individuals at each time step t and region r in constraint (3). The weekly movement rate are shown in Table 7. The expression $\sum_{r' \in \mathcal{R}} \nu_{r' \rightarrow r} S_{\omega,t,r'} - \sum_{r' \in \mathcal{R}} \nu_{r \rightarrow r'} S_{\omega,t,r}$ represents the net movement of susceptible individuals between regions. Since most migration occurs within regions, the flow between regions has a negligible impact on the model.

Figure 14: County and regional migration patterns in Arkansas: Analyzing annual inter-county flows and aggregate regional migration trends.



Appendix G Model Data

Table 8 presents the parameter values used in the proposed compartmental MSP model. Table 9 details the parameter values for the four different regions included in the study. The upper portion of the table includes the tuned parameters derived from the calibration process, which is described in Section 4.2.

Table 8: Parameter values used in the proposed model.

Parameter	Value	Source	Parameter	Value	Source
$ \mathcal{T} $	20		$\gamma^s, \gamma^{ks}, \gamma^c$	0.637, 0.233, 0.333	[Zhou et al., 2020b]
$ \mathcal{R} $	4		μ^{ks}	1.000	
$ \Omega $	81		p^m, p^s, p^c	0.800, 0.150, 0.050	[Wu and McGoogan, 2020]
\mathcal{J}	{1, 5, 9, 13, 17}		$p^{r,v}, p^{m,v}, p^{s,v}$	0.850, 0.100, 0.050	[Barnes and Others, 2023]
ϵ	0.950	[Katella, 2023]	ζ^{ks}	0.400	
γ^v	1.000		ζ^c	0.510	[Wu and McGoogan, 2020]

Table 9: Parameter values for each region used in the proposed model.

Parameter	Region (r)			
	R1	R2	R3	R4
$\beta_r^{(1)}$	1.873	2.162	1.805	1.781
$\rho_r^{(1)}$	0.051	0.051	0.043	0.050
$\gamma_r^m^{(1)}$	0.704	0.704	0.704	0.699
$\sigma_r^{(1)}$	0.943	0.877	0.952	0.901
$S_{0,r}^{(1)}$	299,000	1,107,000	129,000	502,000
$E_{0,r}^{(1)}$	3,100	3,200	100	3,500
$I_{0,r}^m^{(1)}$	200	5,900	1,300	3,600
$I_{0,r}^s^{(1)}$	2,500	1,470	80	60
b_r	1,405	9,357	490	2,032
$\mathcal{X}_{0,r}$	77	566	18	105
$n_r / \sum n_r$	0.145	0.568	0.063	0.224

⁽¹⁾ Tuned parameters using Optuna framework, an open-source optimization library that automates hyperparameter tuning.

References

- Karla Therese L. Sy, Laura F. White, and Brooke E. Nichols. Population density and basic reproductive number of COVID-19 across united states counties. *PLOS ONE*, 16:e0249271, 4 2021. ISSN 1932-6203. doi:10.1371/journal.pone.0249271.
- Seyed M Moghadas, Thomas N Vilches, Kevin Zhang, Chad R Wells, Affan Shoukat, Burton H Singer, Lauren Ancel Meyers, Kathleen M Neuzil, Joanne M Langley, Meagan C Fitzpatrick, and Alison P Galvani. The impact of vaccination on Coronavirus disease 2019 (COVID-19) outbreaks in the United States. *Clinical Infectious Diseases*, 73:2257–2264, 12 2021. ISSN 1058-4838. doi:10.1093/cid/ciab079.
- John T. Brooks and Jay C. Butler. Effectiveness of mask wearing to control community spread of SARS-CoV-2. *JAMA*, 325:998, 3 2021. ISSN 0098-7484. doi:10.1001/jama.2021.1505.
- Derek K Chu, Elie A Akl, Stephanie Duda, Karla Solo, Sally Yaacoub, Holger J Schünemann, Derek K Chu, Elie A Akl, Amena El-harakeh, Antonio Bognanni, Tamara Lotfi, Mark Loeb, Anisa Hajizadeh, Anna Bak, Ariel Izcovich, Carlos A Cuello-Garcia, Chen Chen, David J Harris, Ewa Borowiack, Fatimah Chamseddine, Finn Schünemann, Gian Paolo Morgano, Giovanna E U Muti Schünemann, Guang Chen, Hong Zhao, Ignacio Neumann, Jeffrey Chan, Joanne Khabsa, Layal Hneiny, Leila Harrison, Maureen Smith, Nesrine Rizk, Paolo Giorgi Rossi, Pierre AbiHanna, Rayane El-khoury, Rosa Stalteri, Tejan Baldeh, Thomas Piggott, Yuan Zhang, Zahra Saad, Assem Khamis, Marge Reinap, Stephanie Duda, Karla Solo, Sally Yaacoub, and Holger J Schünemann. Physical distancing, face masks, and eye protection to prevent person-to-person transmission of SARS-CoV-2 and COVID-19: a systematic review and meta-analysis. *The Lancet*, 395:1973–1987, 6 2020. ISSN 01406736. doi:10.1016/S0140-6736(20)31142-9.
- Emanuele Blasioli, Bahareh Mansouri, Srinivas Subramanya Tamvada, and Elkafi Hassini. Vaccine allocation and distribution: A review with a focus on quantitative methodologies and application to equity, hesitancy, and COVID-19 pandemic. *Operations Research Forum*, 4:27, 3 2023. ISSN 2662-2556. doi:10.1007/s43069-023-00194-8.
- William Ogilvy Kermack, A. G. McKendrick, and Gilbert Thomas Walker. A contribution to the mathematical theory of epidemics. *Proceedings of the Royal Society of London. Series A, Containing Papers of a Mathematical and Physical Character*, 115(772):700–721, 1927. doi:10.1098/rspa.1927.0118.

- Lingcai Kong, Mengwei Duan, Jin Shi, Jie Hong, Zhaorui Chang, and Zhijie Zhang. Compartmental structures used in modeling COVID-19: a scoping review. *Infectious Diseases of Poverty*, 11:72, 6 2022. ISSN 2049-9957. doi:10.1186/s40249-022-01001-y.
- Yue Xiang, Yonghong Jia, Linlin Chen, Lei Guo, Bizhen Shu, and Enshen Long. COVID-19 epidemic prediction and the impact of public health interventions: A review of COVID-19 epidemic models. *Infectious Disease Modelling*, 6:324–342, 2021. ISSN 24680427. doi:10.1016/j.idm.2021.01.001.
- Bruno Buonomo, Rossella Della Marca, Alberto d’Onofrio, and Maria Groppi. A behavioural modelling approach to assess the impact of COVID-19 vaccine hesitancy. *Journal of Theoretical Biology*, 534:110973, 2 2022. ISSN 00225193. doi:10.1016/j.jtbi.2021.110973.
- Daniela Olivera Mesa, Peter Winskill, Azra C Ghani, and Katharina Hauck. The societal cost of vaccine refusal: A modelling study using measles vaccination as a case study. *Vaccine*, 41:4129–4137, 6 2023. ISSN 0264410X. doi:10.1016/j.vaccine.2023.05.039.
- Sanjay Mehrotra, Hamed Rahimian, Masoud Barah, Fengqiao Luo, and Karolina Schantz. A model of supply-chain decisions for resource sharing with an application to ventilator allocation to combat COVID-19. *Naval Research Logistics (NRL)*, 67:303–320, 8 2020. ISSN 0894-069X. doi:10.1002/nav.21905.
- Sivasubramaniam V Bhavani, Yuan Luo, William D Miller, Lazaro N Sanchez-Pinto, Xuan Han, Chengsheng Mao, Burhaneddin Sandıkçı, Monica E Peek, Craig M Coopersmith, Kelly N Michelson, and William F Parker. Simulation of ventilator allocation in critically ill patients with COVID-19. *American journal of respiratory and critical care medicine*, 204:1224–1227, 11 2021. ISSN 1535-4970. doi:10.1164/rccm.202106-1453LE.
- Lisa M. Koonin, Satish Pillai, Emily B. Kahn, Danielle Moulia, and Anita Patel. Strategies to inform allocation of stockpiled ventilators to healthcare facilities during a pandemic. *Health Security*, 18:69–74, 4 2020. ISSN 2326-5094. doi:10.1089/hs.2020.0028.
- Dimitris Bertsimas, Leonard Boussieux, Ryan Cory-Wright, Arthur Delarue, Vassilis Digalakis, Alexandre Jacquillat, Driss Lahlou Kitane, Galit Lukin, Michael Li, Luca Mingardi, Omid Nohadani, Agni Orfanoudaki, Theodore Papalexopoulos, Ivan Paskov, Jean Pauphilet, Omar Skali Lami, Bartolomeo Stellato, Hamza Tazi Bouardi, Kimberly Villalobos Carballo, Holly Wiberg, and Cynthia Zeng. From predictions to prescriptions: A data-driven response to COVID-19. *Health Care Management Science*, 24:253–272, 6 2021. ISSN 1386-9620. doi:10.1007/s10729-020-09542-0.
- John R Birge and Francois Louveaux. *Introduction to stochastic programming*. Springer Science & Business Media, 2011.
- Xuecheng Yin and I. Esra Buyuktahtakin. A multi-stage stochastic programming approach to epidemic resource allocation with equity considerations. *Health Care Management Science*, 24:597–622, 9 2021a. ISSN 1386-9620. doi:10.1007/s10729-021-09559-z.
- Xuecheng Yin, I. Esra Buyuktahtakin, and Bhumi P. Patel. COVID-19: Data-driven optimal allocation of ventilator supply under uncertainty and risk. *European Journal of Operational Research*, 304:255–275, 1 2023. ISSN 03772217. doi:10.1016/j.ejor.2021.11.052.
- Reed Albergotti and Faiz Siddiqui. Ford and GM are racing to build coronavirus ventilators, but their efforts may be too late, 04 2020. URL <https://www.washingtonpost.com/business/2020/04/04/ventilators-coronavirus-ford-gm/>. (Accessed on 2023-10-23).
- Vaibhav Mishra, Golnoush Seyedzenouzi, Ahmad Almohtadi, Tasnim Chowdhury, Arwa Khashkhasha, Ariana Axiq, Wing Yan Elizabeth Wong, and Amer Harky. Health inequalities during COVID-19 and their effects on morbidity and mortality. *Journal of Healthcare Leadership*, Volume 13:19–26, 1 2021. ISSN 1179-3201. doi:10.2147/JHL.S270175.
- Joseph T Wu, Kathy Leung, and Gabriel M Leung. Nowcasting and forecasting the potential domestic and international spread of the 2019-nCoV outbreak originating in Wuhan, China: a modelling study. *The Lancet*, 395:689–697, 2 2020. ISSN 01406736. doi:10.1016/S0140-6736(20)30260-9.
- Aniruddha Adiga, Devdatt Dubhashi, Bryan Lewis, Madhav Marathe, Srinivasan Venkatramanan, and Anil Vullikanti. Mathematical models for COVID-19 pandemic: A comparative analysis. *Journal of the Indian Institute of Science*, 100:793–807, 10 2020. ISSN 0970-4140. doi:10.1007/s41745-020-00200-6.
- Alexander Rodríguez, Anika Tabassum, Jiaming Cui, Jiajia Xie, Javen Ho, Pulak Agarwal, Bijaya Adhikari, and B. Aditya Prakash. DeepCOVID: An operational deep learning-driven framework for explainable real-time COVID-19 forecasting. *Proceedings of the AAAI Conference on Artificial Intelligence*, 35:15393–15400, 5 2021. ISSN 2374-3468. doi:10.1609/aaai.v35i17.17808.

- Tao Zhou, Quanhui Liu, Zimo Yang, Jingyi Liao, Kexin Yang, Wei Bai, Xin Lu, and Wei Zhang. Preliminary prediction of the basic reproduction number of the Wuhan novel coronavirus 2019-nCoV. *Journal of Evidence-Based Medicine*, 13:3–7, 2 2020a. ISSN 1756-5383. doi:10.1111/jebm.12376.
- Meng-Chun Chang, Rebecca Kahn, Yu-An Li, Cheng-Sheng Lee, Caroline O. Buckee, and Hsiao-Han Chang. Variation in human mobility and its impact on the risk of future COVID-19 outbreaks in Taiwan. *BMC Public Health*, 21:226, 12 2021a. ISSN 1471-2458. doi:10.1186/s12889-021-10260-7.
- Cliff C. Kerr, Robyn M. Stuart, Dina Mistry, Romesh G. Abeysuriya, Katherine Rosenfeld, Gregory R. Hart, Rafael C. Núñez, Jamie A. Cohen, Prashanth Selvaraj, Brittany Hagedorn, Lauren George, Michał Jastrzębski, Amanda S. Izzo, Greer Fowler, Anna Palmer, Dominic Delpont, Nick Scott, Sherrie L. Kelly, Caroline S. Bennette, Bradley G. Wagner, Stewart T. Chang, Assaf P. Oron, Edward A. Wenger, Jasmina Panovska-Griffiths, Michael Famulare, and Daniel J. Klein. Covasim: An agent-based model of COVID-19 dynamics and interventions. *PLOS Computational Biology*, 17:e1009149, 7 2021. ISSN 1553-7358. doi:10.1371/journal.pcbi.1009149.
- Serina Chang, Emma Pierson, Pang Wei Koh, Jaline Gerardin, Beth Redbird, David Grusky, and Jure Leskovec. Mobility network models of COVID-19 explain inequities and inform reopening. *Nature*, 589:82–87, 1 2021b. ISSN 0028-0836. doi:10.1038/s41586-020-2923-3.
- Mark Kimathi, Samuel Mwalili, Viona Ojiambo, and Duncan Kioi Gathungu. Age-structured model for COVID-19: Effectiveness of social distancing and contact reduction in kenya. *Infectious Disease Modelling*, 6:15–23, 2021. ISSN 24680427. doi:10.1016/j.idm.2020.10.012.
- Ashleigh R. Tuite, David N. Fisman, and Amy L. Greer. Mathematical modelling of COVID-19 transmission and mitigation strategies in the population of ontario, canada. *Canadian Medical Association Journal*, 192:E497–E505, 5 2020. ISSN 0820-3946. doi:10.1503/cmaj.200476.
- Brody H. Foy, Brian Wahl, Kayur Mehta, Anita Shet, Gautam I. Menon, and Carl Britto. Comparing COVID-19 vaccine allocation strategies in india: A mathematical modelling study. *International Journal of Infectious Diseases*, 103:431–438, 2 2021. ISSN 12019712. doi:10.1016/j.ijid.2020.12.075.
- Phenyo E. Lekone and Bärbel F. Finkenstädt. Statistical inference in a stochastic epidemic SEIR model with control intervention: Ebola as a case study. *Biometrics*, 62:1170–1177, 12 2006. ISSN 0006-341X. doi:10.1111/j.1541-0420.2006.00609.x.
- A. Gray, D. Greenhalgh, L. Hu, X. Mao, and J. Pan. A stochastic differential equation SIS epidemic model. *SIAM Journal on Applied Mathematics*, 71:876–902, 1 2011. ISSN 0036-1399. doi:10.1137/10081856X.
- Davide Faranda and Tommaso Alberti. Modeling the second wave of COVID-19 infections in France and Italy via a stochastic SEIR model. *Chaos: An Interdisciplinary Journal of Nonlinear Science*, 30, 11 2020. ISSN 1054-1500. doi:10.1063/5.0015943.
- Tapiwa Ganyani, Christel Faes, and Niel Hens. Simulation and analysis methods for stochastic compartmental epidemic models. *Annual Review of Statistics and Its Application*, 8:69–88, 3 2021. ISSN 2326-8298. doi:10.1146/annurev-statistics-061120-034438.
- Alexander V. Maltsev and Michael D. Stern. Social heterogeneity drives complex patterns of the COVID-19 pandemic: Insights from a novel stochastic heterogeneous epidemic model (SHEM). *Frontiers in Physics*, 8, 1 2021. ISSN 2296-424X. doi:10.3389/fphy.2020.609224.
- Marino Gatto, Enrico Bertuzzo, Lorenzo Mari, Stefano Miccoli, Luca Carraro, Renato Casagrandi, and Andrea Rinaldo. Spread and dynamics of the COVID-19 epidemic in Italy: Effects of emergency containment measures. *Proceedings of the National Academy of Sciences*, 117:10484–10491, 5 2020. ISSN 0027-8424. doi:10.1073/pnas.2004978117.
- Giulia Giordano, Franco Blanchini, Raffaele Bruno, Patrizio Colaneri, Alessandro Di Filippo, Angela Di Matteo, and Marta Colaneri. Modelling the COVID-19 epidemic and implementation of population-wide interventions in Italy. *Nature Medicine*, 26:855–860, 6 2020. ISSN 1078-8956. doi:10.1038/s41591-020-0883-7.
- Mirjam E Kretzschmar, Ganna Rozhnova, Martin C J Bootsma, Michiel van Boven, Janneke H H M van de Wijkert, and Marc J M Bonten. Impact of delays on effectiveness of contact tracing strategies for COVID-19: a modelling study. *The Lancet Public Health*, 5:e452–e459, 8 2020. ISSN 24682667. doi:10.1016/S2468-2667(20)30157-2.
- Adam J Kucharski, Timothy W Russell, Charlie Diamond, Yang Liu, John Edmunds, Sebastian Funk, Rosalind M Eggo, Fiona Sun, Mark Jit, James D Munday, Nicholas Davies, Amy Gimma, Kevin van Zandvoort, Hamish Gibbs, Joel Hellewell, Christopher I Jarvis, Sam Clifford, Billy J Quilty, Nikos I Bosse, Sam Abbott, Petra Klepac, and Stefan Flasche. Early dynamics of transmission and control of COVID-19: a mathematical modelling study. *The Lancet Infectious Diseases*, 20:553–558, 5 2020. ISSN 14733099. doi:10.1016/S1473-3099(20)30144-4.

- WHO. Ten threats to global health in 2019, 2019. <https://www.who.int/news-room/spotlight/ten-threats-to-global-health-in-2019> (Accessed on 21/06-14).
- Wongyeong Choi and Eunha Shim. Optimal strategies for vaccination and social distancing in a game-theoretic epidemiologic model. *Journal of Theoretical Biology*, 505:110422, 11 2020. ISSN 00225193. doi:10.1016/j.jtbi.2020.110422.
- Susanne F. Awad, Godfrey Musuka, Zindoga Mukandavire, Dillon Froass, Neil J. MacKinnon, and Diego F. Cuadros. Implementation of a vaccination program based on epidemic geospatial attributes: COVID-19 pandemic in Ohio as a case study and proof of concept. *Vaccines*, 9:1242, 10 2021. ISSN 2076-393X. doi:10.3390/vaccines9111242.
- Shuanglin Jing, Russell Milne, Hao Wang, and Ling Xue. Vaccine hesitancy promotes emergence of new SARS-CoV-2 variants. *Journal of Theoretical Biology*, 570:111522, 8 2023. ISSN 00225193. doi:10.1016/j.jtbi.2023.111522.
- Hieu Bui, Sandra Eksioglou, and Ruben Proano. Evaluating the impact of vaccine hesitancy on the allocation of vital resources during COVID-19 pandemic, 03 2024. URL arXiv:2403.07971. (Accessed on 3/15/2024).
- Adam F. Abidin, Yi-Ping Fang, Aakil Caunhye, Douglas Alem, Anne Barros, and Enrico Zio. An optimization model for planning testing and control strategies to limit the spread of a pandemic – the case of COVID-19. *European Journal of Operational Research*, 304:308–324, 1 2023. ISSN 03772217. doi:10.1016/j.ejor.2021.10.062.
- M. V. F. Pereira and L. M. V. G. Pinto. Multi-stage stochastic optimization applied to energy planning. *Mathematical Programming*, 52:359–375, 5 1991. ISSN 0025-5610. doi:10.1007/BF01582895.
- Mark Goh, Joseph Y.S. Lim, and Fanwen Meng. A stochastic model for risk management in global supply chain networks. *European Journal of Operational Research*, 182:164–173, 10 2007. ISSN 03772217. doi:10.1016/j.ejor.2006.08.028.
- Sizhe Zhang and Michel-Alexandre Cardin. Flexibility and real options analysis in emergency medical services systems using decision rules and multi-stage stochastic programming. *Transportation Research Part E: Logistics and Transportation Review*, 107:120–140, 11 2017. ISSN 13665545. doi:10.1016/j.tre.2017.09.003.
- Can Li and Ignacio E. Grossmann. A review of stochastic programming methods for optimization of process systems under uncertainty. *Frontiers in Chemical Engineering*, 2, 1 2021. ISSN 2673-2718. doi:10.3389/fceng.2020.622241.
- Gilbert Laporte and François V. Louveaux. The integer L-shaped method for stochastic integer programs with complete recourse. *Operations Research Letters*, 13:133–142, 4 1993. ISSN 01676377. doi:10.1016/0167-6377(93)90002-X.
- Monique Guignard. Lagrangean relaxation. *Top*, 11:151–200, 12 2003. ISSN 1134-5764. doi:10.1007/BF02579036.
- Brianna Christian and Selen Cremaschi. Heuristic solution approaches to the pharmaceutical R&D pipeline management problem. *Computers & Chemical Engineering*, 74:34–47, 3 2015. ISSN 00981354. doi:10.1016/j.compchemeng.2014.12.014.
- Xuecheng Yin and I. Esra Buyuktahtakin. Risk-averse multi-stage stochastic programming to optimizing vaccine allocation and treatment logistics for effective epidemic response. *medRxiv*, 2021b. doi:10.1101/2021.05.28.21258003.
- Seyyed-Mahdi Hosseini-Motlagh, Mohammad Reza Ghatreh Samani, and Shamim Homaei. Design of control strategies to help prevent the spread of COVID-19 pandemic. *European Journal of Operational Research*, 304:219–238, 1 2023. ISSN 03772217. doi:10.1016/j.ejor.2021.11.016.
- Matthew W. Tanner, Lisa Sattenspiel, and Lewis Ntamo. Finding optimal vaccination strategies under parameter uncertainty using stochastic programming. *Mathematical Biosciences*, 215:144–151, 10 2008. ISSN 00255564. doi:10.1016/j.mbs.2008.07.006.
- Hamed Yarmand, Julie S. Ivy, Brian Denton, and Alun L. Lloyd. Optimal two-phase vaccine allocation to geographically different regions under uncertainty. *European Journal of Operational Research*, 233:208–219, 2 2014. ISSN 03772217. doi:10.1016/j.ejor.2013.08.027.
- WHO. Guidance on ethics and equitable access to HIV treatment and care. <https://www.who.int/publications/i/item/9241592583>, June 2004. (Accessed on 03/15/2024).
- Haylee Lane, Mitchell Sarkies, Jennifer Martin, and Terry Haines. Equity in healthcare resource allocation decision making: A systematic review. *Social Science & Medicine*, 175:11–27, 2 2017. ISSN 02779536. doi:10.1016/j.socscimed.2016.12.012.
- Li Sun, Gail W. DePuy, and Gerald W. Evans. Multi-objective optimization models for patient allocation during a pandemic influenza outbreak. *Computers & Operations Research*, 51:350–359, 11 2014. ISSN 03050548. doi:10.1016/j.cor.2013.12.001.
- Ming Liu, Zhe Zhang, and Ding Zhang. A dynamic allocation model for medical resources in the control of influenza diffusion. *Journal of Systems Science and Systems Engineering*, 24:276–292, 9 2015. ISSN 1004-3756. doi:10.1007/s11518-015-5276-y.

- Ming Liu and Ding Zhang. A dynamic logistics model for medical resources allocation in an epidemic control with demand forecast updating. *Journal of the Operational Research Society*, 67:841–852, 6 2016. ISSN 0160-5682. doi:10.1057/jors.2015.105.
- Gregory S. Zaric and Margaret L. Brandeau. Resource allocation for epidemic control over short time horizons. *Mathematical Biosciences*, 171:33–58, 5 2001. ISSN 00255564. doi:10.1016/S0025-5564(01)00050-5.
- R. Thomas Day, Bradley S. Guidry, Brian C. Drolet, and Ellen W. Clayton. From ventilators to vaccines: Reframing the ethics of resource allocation. *The American Journal of Bioethics*, 20:W15–W16, 7 2020. ISSN 1526-5161. doi:10.1080/15265161.2020.1782530.
- Irem Sengul Orgut, Julie Ivy, Reha Uzsoy, and James R. Wilson. Modeling for the equitable and effective distribution of donated food under capacity constraints. *IIE Transactions*, 48:252–266, 3 2016. ISSN 0740-817X. doi:10.1080/0740817X.2015.1063792.
- Ashley E. Davis, Sanjay Mehrotra, John J. Friedewald, Mark S. Daskin, Anton I. Skaro, Michael M. Abecassis, and Daniela P. Ladner. Improving geographic equity in kidney transplantation using alternative kidney sharing and optimization modeling. *Medical Decision Making*, 35:797–807, 8 2015. ISSN 0272-989X. doi:10.1177/0272989X14557696.
- Zehranaz Dönmez, Serkan Turhan, Özlem Karsu, Bahar Y. Kara, and Oya Karaşan. Fair allocation of personal protective equipment to health centers during early phases of a pandemic. *Computers & Operations Research*, 141:105690, 5 2022. ISSN 03050548. doi:10.1016/j.cor.2021.105690.
- Joshua A. Salomon, Alex Reinhart, Alyssa Bilinski, Eu Jing Chua, Wichada La Motte-Kerr, Minttu M. Rönn, Marissa B. Reitsma, Katherine A. Morris, Sarah LaRocca, Tamer H. Farag, Frauke Kreuter, Roni Rosenfeld, and Ryan J. Tibshirani. The US COVID-19 Trends and Impact Survey: Continuous real-time measurement of COVID-19 symptoms, risks, protective behaviors, testing, and vaccination. *Proceedings of the National Academy of Sciences*, 118(51):e2111454118, 2021.
- CDC. COVID-19 vaccinations in the United States, county, 2021. URL <https://data.cdc.gov/Vaccinations/COVID-19-Vaccinations-in-the-United-States-County/8xxk-amqh>. (Accessed on 2021-12-25).
- Benjamin Wacker and Jan Schlüter. Time-continuous and time-discrete SIR models revisited: theory and applications. *Advances in Difference Equations*, 2020(1):556, 2020.
- Ciara E. Dangerfield, Martin Vyska, and Christopher A. Gilligan. Resource allocation for epidemic control across multiple sub-populations. *Bulletin of Mathematical Biology*, 81:1731–1759, 6 2019. ISSN 0092-8240. doi:10.1007/s11538-019-00584-2.
- World Health Organization. A global framework to ensure equitable and fair allocation of COVID-19 products and potential implications for COVID-19 vaccination. Technical report, World Health Organization, 2020. URL https://apps.who.int/gb/COVID-19/pdf_files/02_07/Global_Allocation_Framework.pdf. Accessed: 2024-02-24.
- CovidCareMap. COVID-19 health system capacity. <https://github.com/covidcaremap/covid19-healthsystemcapacity/tree/master/data/published>, 2020. URL <https://github.com/covidcaremap/covid19-healthsystemcapacity/tree/master/data/published>. Accessed: 2024-01-12.
- Pauli Virtanen, Ralf Gommers, Travis E. Oliphant, Matt Haberland, Tyler Reddy, David Cournapeau, Evgeni Burovski, Pearu Peterson, Warren Weckesser, Jonathan Bright, Stéfan J. van der Walt, Matthew Brett, Joshua Wilson, K. Jarrod Millman, Nikolay Mayorov, Andrew R. J. Nelson, Eric Jones, Robert Kern, Eric Larson, C J Carey, İlhan Polat, Yu Feng, Eric W. Moore, Jake VanderPlas, Denis Laxalde, Josef Perktold, Robert Cimrman, Ian Henriksen, E. A. Quintero, Charles R. Harris, Anne M. Archibald, Antônio H. Ribeiro, Fabian Pedregosa, Paul van Mulbregt, and SciPy 1.0 Contributors. SciPy 1.0: Fundamental Algorithms for Scientific Computing in Python. *Nature Methods*, 17:261–272, 2020. doi:10.1038/s41592-019-0686-2.
- Delano Massey and Devan Cole. HHS to work with GM under Defense Production Act to produce 30,000 ventilators for national stockpile | cnn politics, 04 2020. URL <https://www.cnn.com/2020/04/08/politics/general-motors-ventilators-defense-production-act-coronavirus/index.html>. (Accessed on 10/06/2023).
- AdvaMed. Tens of thousands of life-saving ventilators on deck to combat COVID-19 - advamed, 04 2020. URL <https://www.advamed.org/industry-updates/news/tens-of-thousands-of-life-saving-ventilators-on-deck-to-combat-covid-19/>. (Accessed on 11/06/2023).
- O. Wahltinez et al. COVID-19 Open-Data: curating a fine-grained, global-scale data repository for SARS-CoV-2. 2020. URL <https://goo.gle/covid-19-open-data>.

- Takuya Akiba, Shotaro Sano, Toshihiko Yanase, Takeru Ohta, and Masanori Koyama. Optuna: A next-generation hyperparameter optimization framework. In *Proceedings of the 25th ACM SIGKDD International Conference on Knowledge Discovery and Data Mining*, 2019.
- Laureano Escudero, Araceli Garín, María Merino, and Gloria Pérez. The value of the stochastic solution in multistage problems. *TOP: An Official Journal of the Spanish Society of Statistics and Operations Research*, 15:48–64, 02 2007.
- U.S. Census Bureau. County-to-county migration flows: 2016-2020 acs. <https://www.census.gov/data/tables/2020/demo/geographic-mobility/county-to-county-migration-2016-2020.html>, 2020. Accessed: 2024-01-12.
- Fei Zhou, Ting Yu, Ronghui Du, Guohui Fan, Ying Liu, Zhibo Liu, Jie Xiang, Yeming Wang, Bin Song, Xiaoying Gu, Lulu Guan, Yuan Wei, Hui Li, Xudong Wu, Jiuyang Xu, Shengjin Tu, Yi Zhang, Hua Chen, and Bin Cao. Clinical course and risk factors for mortality of adult inpatients with COVID-19 in Wuhan, China: a retrospective cohort study. *The Lancet*, 395:1054–1062, 3 2020b. ISSN 01406736. doi:10.1016/S0140-6736(20)30566-3.
- Zunyou Wu and Jennifer M. McGoogan. Characteristics of and important lessons from the Coronavirus disease 2019 (COVID-19) outbreak in China. *JAMA*, 323:1239, 4 2020. ISSN 0098-7484. doi:10.1001/jama.2020.2648.
- Eleanor Barnes and Others. SARS-CoV-2-specific immune responses and clinical outcomes after COVID-19 vaccination in patients with immune-suppressive disease. *Nature Medicine*, 29:1760–1774, 7 2023. ISSN 1078-8956. doi:10.1038/s41591-023-02414-4.
- Kathy Katella. Comparing the COVID-19 vaccines: How are they different? <https://www.yalemedicine.org/news/covid-19-vaccine-comparison>, 10 2023. (Accessed on 01/13/2024).